SEARCH FOR RESONANT DOUBLE HIGGS PRODUCTION WITH bbZZ DECAYS IN THE $b\bar{b}\ell\ell\nu\bar{\nu}$ FINAL STATE IN pp COLLISIONS AT $\sqrt{s} = 13$ TeV

by

Rami Kamalieddin

A DISSERTATION

Presented to the Faculty of

The Graduate College at the University of Nebraska

In Partial Fulfilment of Requirements

For the Degree of Doctor of Philosophy

Major: Physics and Astronomy

Under the Supervision of Professor Ilya Kravchenko

Lincoln, Nebraska

May, 2019

SEARCH FOR RESONANT DOUBLE HIGGS PRODUCTION WITH bbZZ DECAYS IN THE $b\bar{b}\ell\ell\nu\bar{\nu}$ FINAL STATE IN pp COLLISIONS AT $\sqrt{s} = 13$ TeV

Rami Kamalieddin, Ph.D.

University of Nebraska, 2019

Adviser: Ilya Kravchenko

Since the discovery of the Higgs boson in 2012 by the ATLAS and CMS experiments, most of the quantum mechanical properties that describe the long-awaited Higgs boson have been measured. Due to the outstanding work of the LHC, over a hundred of $fb^{-1}$ of data have been delivered to both experiments. Finally, it became sensible for analyses teams to start working with a very low cross section processes, which made it possible to observe rare decay modes of the Higgs boson, e.g., a recent success in observing ttH and VHbb processes. One of the main remaining untouched topics is a double Higgs boson production. However, additional hundred of $fb^{-1}$ per year from the HL-LHC will not necessarily help us much with the SM double Higgs physics, the process may remain unseen even in the most optimistic scenarios. The solution is to work in parallel on new reconstruction and signal extraction methods as well as new analysis techniques to improve the sensitivity of measurements. This thesis is about both approaches: we have used the largest available dataset at the time the analysis has been performed and developed/used the most novel analysis methods. One of such methods is the new electron identification algorithm that we have developed at the CMS electron identification group, to which I have had a privilege to contribute during several years of my stay at CERN.

The majority of this thesis is devoted to techniques for the first search at the LHC for the double Higgs boson production mediated by a heavy narrow-width resonance

in the $b\bar{b}ZZ$ channel: $X \to HH \to b\bar{b}ZZ^* \to b\bar{b}\ell\ell\nu\bar{\nu}$. The measurement searches for a resonant production of a Higgs boson pair in the range of masses of the resonant parent particle from 250 to 1000 GeV using 35.9 $fb^{-1}$ of data taken in 2016 at 13 TeV. Two spin scenarios of the resonance are considered: spin 0 and spin 2. In the absence of the evidence of the resonant double Higgs boson production from the previous searches, we proceed with setting the upper confidence limits.

*"... a place for a smart quote"*

*Lenin, 1922.*

## ACKNOWLEDGMENTS

This will be a long list!

# Table of Contents

# List of Figures

# List of Tables

Chapter *1*

# Introduction

This chapter describes the development of particle physics following the historical order of how particles were discovered and parts of the Standard Model (SM) were constructed.

## 1.1 "All things are made of atoms"

The SM is the theory of particles and their interactions that was built during many decades of intense experimental and theoretical work. Particles in this theory are elementary and have no size, meaning they cannot be divided further. This idea of the point-like particles is crucial since it reflects the goal of particle physics to find and describe the smallest and the most fundamental scale at which nature works. For the last several decades the SM is the most tested theory of elementary particles and forces and is presently generally accepted by the whole physics community. Formally, all SM elementary particles are split into two classes: fermions and bosons. Particles with a half-integer spin 1/2 (quarks and leptons) are called fermions since they obey Fermi-Dirac statistics [1]. The other class of particles is bosons. They are force carriers, have an integer spin, and are characterised by the Bose-Einstein statistics. A rigorous mathematical description of the SM will be given in the next chapter.

Our macroscopic world, from the smallest viruses to the biggest stars, is made of molecules and atoms. To show how deep and significant this simple idea is, let us quote Richard Feynman, a Physics Nobel Prize winner, who once summarised in a single phrase what he believed to be the most important fact about the world around us: "all things are made of atoms" [2]. Feynman himself was the father of quantum electrodynamics, and in this simple statement - delivered originally to Caltech students and now known to everyone through his series of physics books - he decided not to go into quantum mechanics principles and instead illustrated at the rather highly abstract level that everything is made of smaller particles. The quest to the smallest scale and the theory that would describe it were the key ideas that ultimately led to the development of the SM.

Today the physics community knows that molecules are made of atoms, which are not elementary particles either. Instead, atoms have heavy nuclei and light electrons "orbiting" around the nucleus on the electron shells. The nucleus is positively charged proportionally to the number of protons it contains. To provide the stability of the nuclei of the heavy atoms our world also needs neutrons, which have no electric charge. Going to an even smaller scale, it is now known that protons and neutrons are not elementary; rather, they are composed of point-like constituents that are called quarks (see Figure 1.1).

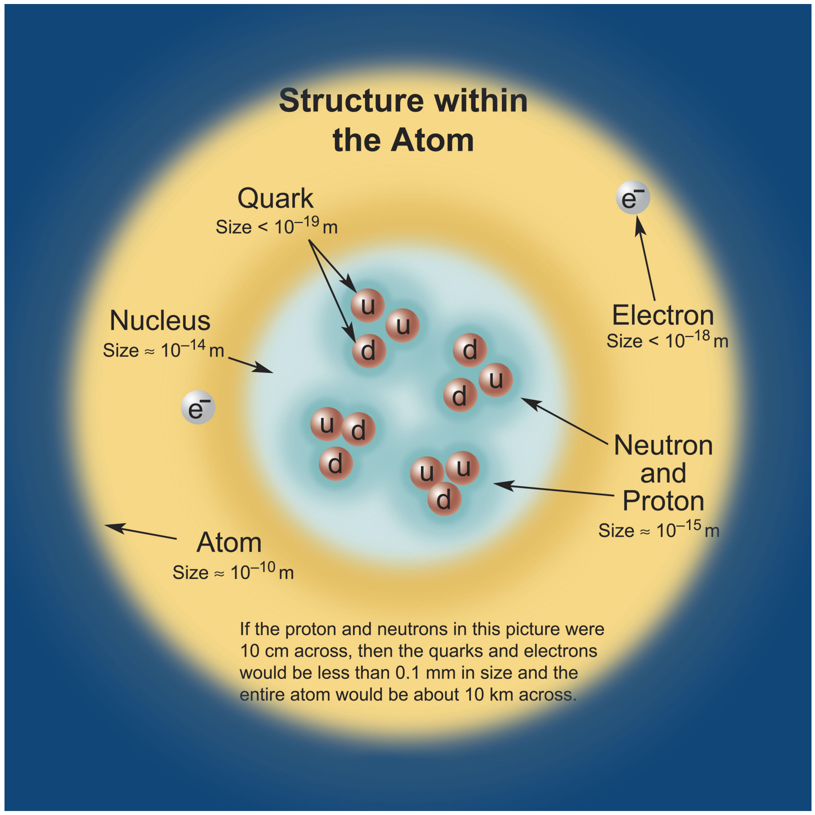


**Figure 1.1:** The structure of an atom. Approximate scale values are indicated.

Quarks were proposed by Gell-Mann and also by Zweig to explain periodicity in properties of observed subatomic particles [3]. Quarks are arranged in three families or three generations of doublets. A doublet is a mathematical construct that is used to explain a two-value system. For example, by design of Gell-Mann and Zweig, each quark doublet in their theory is a two quark system that has an "up" quark with the electric charge $+1/3$ and a "down" quark with the charge $-2/3$. For antiquarks, the signs of the charges are reversed. The physics world before Gell-Mann and Zweig got used to the fact that particles have integer charges due to an enormous number of observations. The fact that the quark charge values were fractional was so revolutionary to Gell-Mann that he decided not to publish his article in a highly prestigious journal but, expecting a rejection, decided to go with a second tier one [3]. However, with time out of all the theories that were trying to explain the difference in masses of observed hadrons it was the hypothesis of Gell-Mann and Zweig that turned out to be correct. Now, the quark theory is one of the key elements of the SM.

The SM includes six different types of quarks: up, down, charm, strange, top, and bottom. To distinguish one quark from another there is a "flavor" number assigned to them. For instance, a charm quark has $+1$ unit of "charmness", while a strange quark has $-1$ unit of "strangeness". All the other flavor fields are zero for quarks. This pattern is applied to all the other four quarks to fill the corresponding "quarkness" numbers. Another important characteristic of quarks was revealed at the $e^+e^-$ colliders when physicists compared production rates of muons and hadrons. The theory was off by a factor of three. This was the motivation to introduce three quark colours: green, blue, and red.

Quarks were observed decades after electrons had been discovered. In particle physics, the electron belongs to a family of leptons. A lepton is an elementary particle with a spin 1/2 that participates in all but strong interactions, which will be discussed in more detail later in this chapter. The electron was discovered by Thompson [4] in 1897 when he was studying the properties of a cathode ray. Due to this discovery, that year may be considered the beginning of an era of a particle physics: dozens of particles were discovered in the next decades. In 1936, another lepton was observed, the muon [5], in an experiment of Anderson and Neddermeyer who studied cosmic radiation. In essence, a muon is almost a copy of an electron, but is 207 times heavier. No explanation for this mass difference exists in the SM. As a side note, according to Carl Bender, there is a story that Feynman was able to derive the mass of the muon starting with the mass of an electron, but the world has never seen that calculation published [6].

Leptons are also arranged in generations, analogously to quark families. Each generation is a doublet that consists of a charged lepton (electron, muon or tau) with the charge $-1$ and a neutral lepton (corresponding electron, muon, or a tau neutrino). Electron and muon neutrinos had been discovered in 1956 and 1962, respectively. The existence of the electron neutrino was deduced from the violation of the conservation of energy in a beta decay. The muon neutrino [7] was discovered by Schwartz, Lederman, and Steinberger during an experiment with a pion beam where leptons from the pion decays arrived to the aluminum spark chamber after passing a steel wall. Fifty-one events of interest had been observed after running the experiment for several months. Those events could not be initiated by electron neutrinos, since they will interact with the metal and produce electrons. The presence of narrow muon tracks in the chamber in each event, hence muons, was a clear indication that those neutrinos were of a different kind - they were muon neutrinos. Finally, a tau lepton and a tau neutrino were discovered in 1975 and 2000 correspondingly [8,9]. With that, all three families of the SM leptons were observed: a long-awaited tau neutrino, which decades ago was theoretically speculated to exist, was finally discovered experimentally. In a like manner to families of quarks, lepton masses grow with each generation, where a tau from the third generation is the heaviest lepton. To classify leptons of different families the lepton numbers were reserved: 1 unit of electron number to an electron and an electron neutrino, 1 unit of muon number to a muon and a muon neutrino, and 1 unit of tau number to a tau and a tau neutrino.

## 1.2 Fundamental forces

In nature there are four fundamental forces: gravitational, weak, electromagnetic, and strong forces. This thesis will classify all four forces [10] in terms of the relative strength, the range that they can cover, the spin of the mediator, and whether the force's nature is attractive, repulsive, or both. This should be taken critically, since this is quite an ambiguous categorisation. It has a deep pedagogical meaning, though, because it helps to illustrate in which regime each of the forces is dominant. According to the world known mathematical physicist Carl Bender, this is of great importance since it is one of the main approaches to solving physics problems: to know which effects are the dominant and which are sub-dominant. This helps to justify what effect can be neglected and what approximation can be used. Thus, it allows the possibility to do calculations for problems where closed-form solutions do not exists, which is almost all the complex phenomena around us [6].

The first force on our list of forces is the gravitational force. This force governs the Universe at the macroscopic level: planets, solar systems, etc. The first theory of gravity was formulated by Newton [11]. Einstein later developed a new theory of gravity (GR). The key difference is that the Newtonian gravity had several "absolutes" that GR does not have: absolute time and space, a preferred separation of spacetime into time and spatial parts, absolute simultaneity, etc. [**?**]. Butterworth gives a good historical perspective in [12]. It is worth noting that the gravitational force is not included in the SM. Attempts are ongoing to expand the SM, e.g., adding the graviton as a mediator, but no real success so far has been achieved to create a renormalizable theory that would combine both the SM and gravity [13]. Surprisingly, gravity is the weakest force - the only reason why the motion of planets and galaxies is governed by gravity is because those are gigantic objects. Gravity effects become the dominant ones at the macroscopic scale because of an enormous number of particles involved in the interaction. If the strength of the strongest force, which is the strong force, is set to 1, then the strength of the gravity will be about $10^{-41}$. It is contemplated that the gravity mediator (the graviton), if it exists, would have a charge of zero, zero mass, spin 2, and should be a stable particle. The gravitational force is of the infinite range and its nature is purely attractive, while the other three forces can exhibit both an attractive and a repulsive behaviour. Einstein's general relativity theory, though not a quantum theory, is the only working theory of gravity as of now.

The next force, the weak force, is mediated by a charged W (charge +1/-1) boson or a neutral Z boson, thus giving name to charged and neutral weak interactions correspondingly. All SM fermions, quarks and leptons, experience the weak force. The relative strength of the weak force is $10^{-16}$ and the range of applicability is $10^{-3}$ fm. All three weak bosons ($W^+$, $W^-$, and Z) have spin 1 and are quite massive: $m_{W^\pm} = 80.385$ GeV and $m_Z = 91.189$ GeV. GeV is the unit of the "natural system of units", in which $\hbar = c = 1$. This system is very popular in the high-energy physics and is widely used in this thesis. Adoption of this system simplifies how many equations look and also makes a fine-structure constant $\alpha \approx 1/137$ dimensionless. Using the natural system of units [14], masses, momenta, and energies are measured in electronvolts (eV), with GeV ($10^9$ eV) and TeV ($10^{12}$ eV) being the most popular units in a modern high-energy physics due to the energy regimes involved.

Charged weak interactions are interesting due to the fact that a primitive interaction vertex can be thought of as a point where a charged lepton is converted to a neutral lepton or vice versa. A good example is a muon decay, which is a conversion of the muon to a muon neutrino with the help of the W boson, which further decays to an electron and a corresponding electron antineutrino. It is worth noting that charged weak interactions do not conserve the flavor of quarks; e.g., members of doublets of the third and the second families can be converted into members of the lower family of quarks. This fact is reflected in the Cabibbo-Kobayashi-Maskawa (CKM) matrix [15]. This matrix describes the strength of the flavor-changing weak interactions. Since diagonal elements of this matrix are less than one and off-diagonal elements are non-zero, the CKM matrix represents a mismatch of quantum states of quarks when they propagate freely and when they take part in the weak interactions. In other words, the CKM matrix with non-zero off-diagonal elements means cross-generation interactions are allowed and this is the information that the CKM matrix quantifies.

$$\begin{pmatrix} |V_{ud}| & |V_{us}| & |V_{ub}| \\ |V_{cd}| & |V_{cs}| & |V_{cb}| \\ |V_{td}| & |V_{ts}| & |V_{tb}| \end{pmatrix} = \begin{pmatrix} 0.97427 \pm 0.00015 & 0.22534 \pm 0.00065 & 0.00351^{+0.00015}_{-0.00014} \\ 0.22520 \pm 0.00065 & 0.97344 \pm 0.00016 & 0.0412^{+0.0011}_{-0.0005} \\ 0.00867^{+0.00029}_{-0.00031} & 0.0404^{+0.0011}_{-0.0005} & 0.999146^{+0.000021}_{-0.000046} \end{pmatrix}. \tag{1.1}$$

The third force, the electromagnetic (EM) force, is one of the main forces that we experience in our everyday life. The reason one can sit in the chair and does not fall further down due to gravity, is that electrons of the body repel electrons of the chair. The relative strength of the EM force is $10^{-3}$ and the range of applicability is infinite. A photon, as the EM force's mediator, has zero mass and spin 1. The theory that describes photon interaction with leptons and quarks is called quantum electrodynamics (QED) and was developed in 1940s and 1950s by Tomonaga, Schwinger, Feynman, and Dyson [16]. Electric charge is conserved in EM interactions and no single photon-to-fermion vertex is possible; there are always two fermions that must be involved.

In the SM several multi-boson vertices are allowed. W and Z bosons that participate in weak interactions can couple to each other, so $WWZ, WWWW$, and $WWZZ$ vertices are possible in the SM. In addition, W bosons can couple to photons, so $\gamma WW$, $\gamma WWZ$, and $WW\gamma\gamma$ vertices are allowed too. Even though Z boson is massive and photon is a massless boson, Z boson has a neutral charge. This makes it possible that any interaction where the photon is a force carrier, can also be mediated by the Z boson.

The strong force, the fourth force of nature, is the strongest known force. Gluons are the carriers of this force and each gluon carries one unit of color and one unit of anticolor. There are nine types of gluons but, technically, the ninth gluon is a color invariant and would give rise to an infinite range of the strong force, which contradicts experiments. That is why modern physics assumes that in our world only eight gluons exist [3, 15]. Gluons carry color charge and, thus, can couple to each other. For several high order processes in quantum chromodynamics (QCD), 3- and 4-gluon vertices have to be introduced to restore gauge invariance and no higher order vertices are required [17].

To summarise the knowledge about the SM forces, one often refers to the Feynman diagram representation [18]. Fig. 1.2 shows all allowed SM particle interactions and corresponding simple vertices.

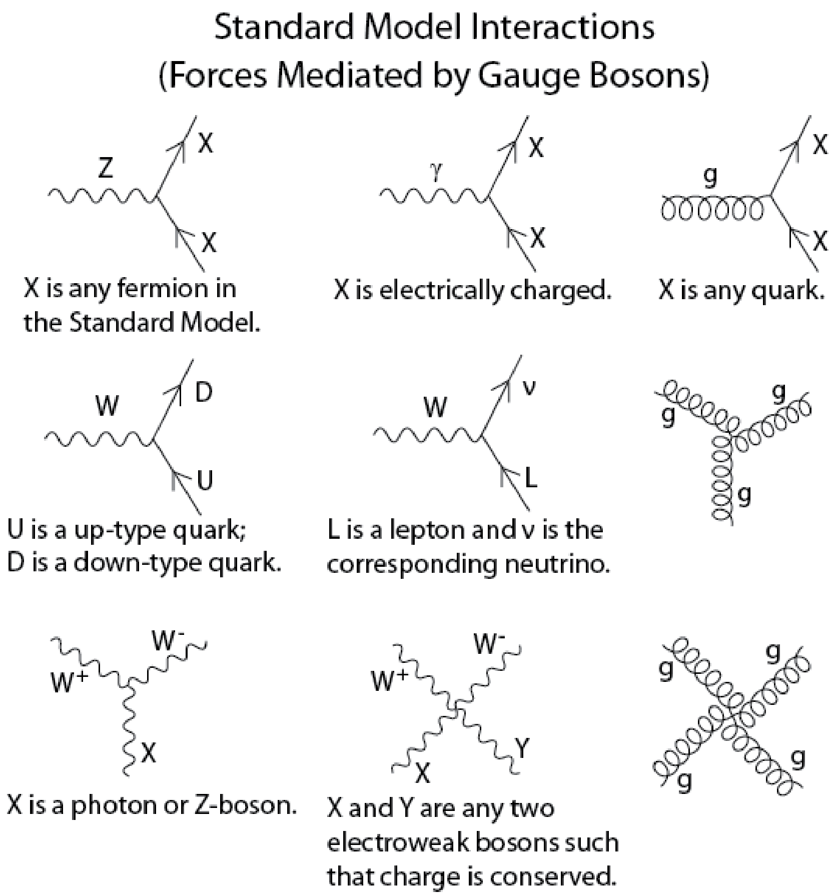


**Figure 1.2:** All SM interaction and simple vertices.

## 1.3 The Brout-Englert-Higgs mechanism

The description of the SM picture will not be complete without mentioning the main particle - the Higgs boson - that was predicted almost 60 years ago, but was not observed yet missing until 2012 (see Fig. 1.3 [19]). After the electroweak (EW) unification by Glashow, Salam, and Weinberg [20], it was still not clear what the origin of the mass of fundamental particles is. In 1964, Robert Brout and François Englert [21], Peter Higgs [22], Gerald Guralnik, C. Richard Hagen, and Tom Kibble [23] (BEHGHK authors), proposed the method by which the particles can acquire mass. This technique consists of three stages and we will discuss them one-by-one:

1. The Brout-Englert-Higgs (BEH) mechanism
2. The BEH field
3. The Higgs boson.

The first stage, the BEH mechanism, is simply a spontaneous symmetry breaking (SSB) mechanism, which is a mathematical trick consisting of rewriting the original scalar fields in the EW Lagrangian, rearranging equations, and requiring that the fields are real. What does this lead to? The BEH authors started with a scalar complex field and a massless vector field and after SSB obtained a single real scalar field (Higgs boson) and a massive vector field. In terms of our physical world this it what gives mass to W and Z bosons.

The second stage is the BEH field. It exists everywhere and has been present almost since the Big Bang [24]. It is a property of our world. All the fundamental particles that interact with the BEH field acquire mass. Those, which do not interact directly (at the tree level) have no mass and all their energy is in the form of the momentum. Such particles can travel with the speed of light. The more the particle interacts with the BEH field, the higher is the coupling to the Higgs boson or simply the higher is the mass of the particle. The coupling of the Higgs boson to fermions is proportional to the mass of the fermions, and for W and Z bosons it is proportional to the squared mass of bosons, making the top quark and the Z boson the most massive fermion and boson respectively (see Fig. 1.4 [25]).

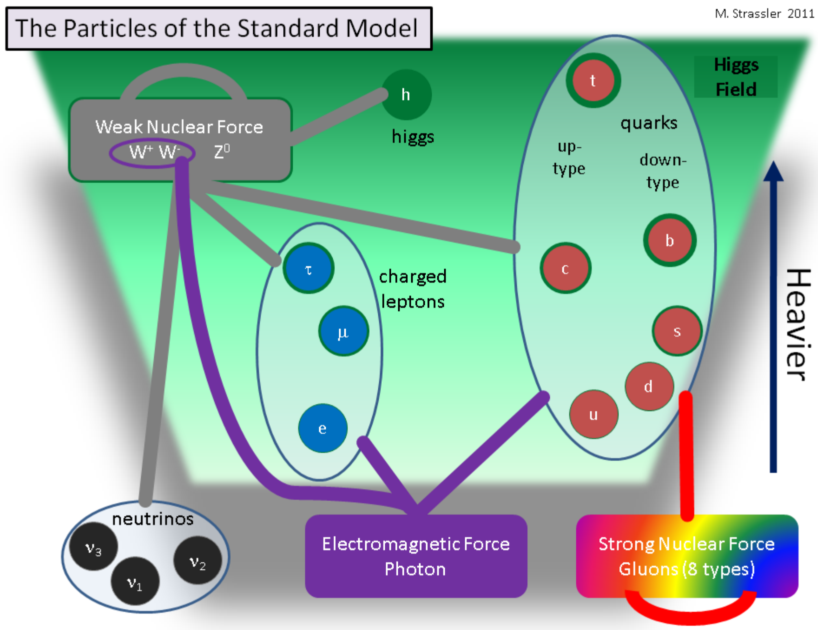


**Figure 1.3:** SM particles and force carriers. Self-interactions are also shown. The strength of the coupling to the Higgs boson increases from the bottom to the top, which is illustrated by the shades of the green color (the Higgs field).

The third and, arguably the most important stage, the Higgs boson. The Higgs boson is the excitation of the BEH field. Thus, the Higgs bosons can be produced at colliders by pumping more and more energy in a small space-time region exciting the BEH field to "produce" the Higgs bosons. In reality this happens through making the LHC beams more energetic and thus, during the collision, producing more energetic gluons (and also more energetic quarks). The main Higgs boson production mechanism is called a gluon fusion, when through the top quark loop a single Higgs boson is produced. This accounts for about 90% of the overall LHC Higgs production at the 13 TeV energy. The second mechanism is a vector boson fusion. The third mechanism is the associated production with a weak boson. The smallest contributor to the Higgs boson production is the $ttH$ process, which stands for the associated production of the Higgs boson with the top anti-top quark pair. All mentioned Higgs boson production mechanisms are presented in the form of Feynman diagrams in Fig. 1.5.

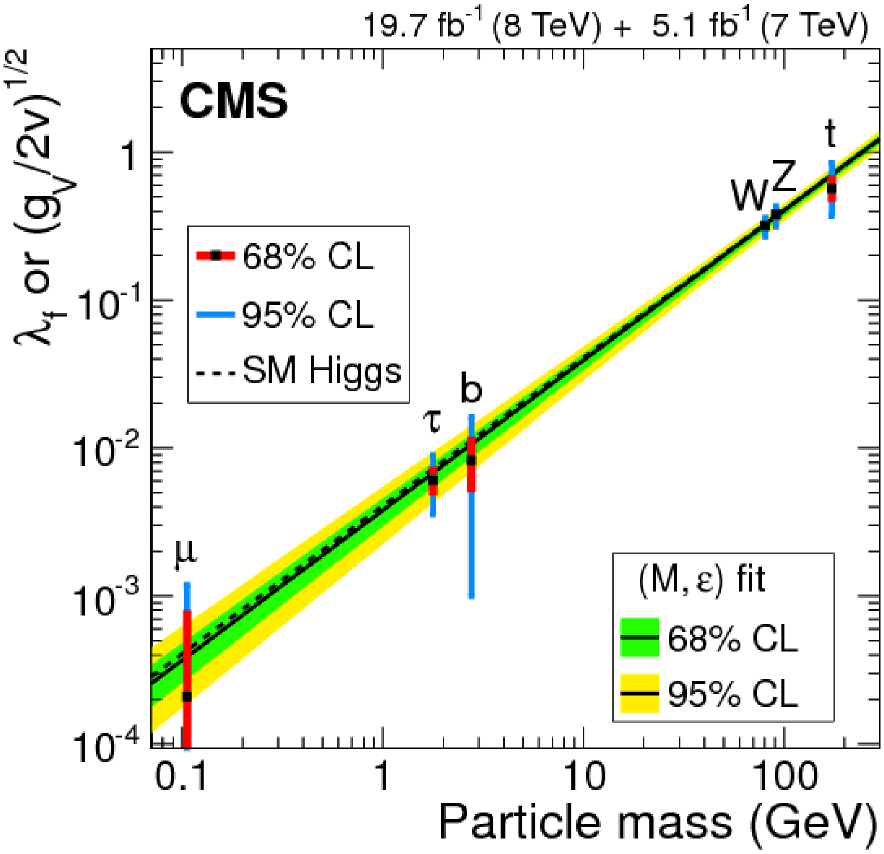


**Figure 1.4:** Coupling of particles to SM Higgs boson versus the mass of the particle, log-log scale is used.

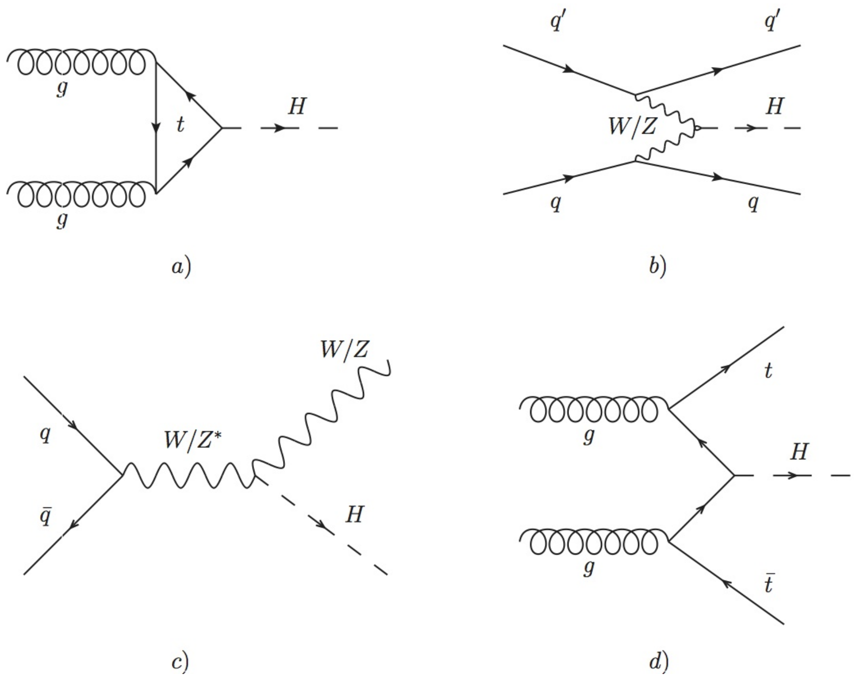


**Figure 1.5:** SM Higgs boson production modes: a) a gluon fashion, b) a vector boson scattering, c) an associated production with a vector boson, d) an associated production with the top anti-top pair.

When describing Higgs bosons physics one cannot avoid mentioning the decay channels of the Higgs boson. In physics branching fraction term is reserved to quantify the probabilities with which a parent particle decays to daughter particles (see Fig. 1.6). The work of this thesis focuses on two specific Higgs boson decays, $H \to b\bar{b}$ and $H \to ZZ$. The first one has the highest branching fraction, while the second one gives a clean signature when subsequent $Z \to \ell\ell$ decays are selected. Before we conclude with the BEHGHK method, a little bit of history, an irony of life, actually. The BEH particle is called the Higgs boson, but Peter Higgs was not the first to publish the article on the BEH mechanism, in fact he was the last out of BEHGHK authors! His very first article was rejected since it contained no specific predictions or conclusions drawn from his calculations. This is why he was out-published by others. But this rejection made him write another article where he explicitly predicted an existence of the new boson. And this is what has made all the difference, he was the first to predict a new boson, and this boson now is called the Higgs boson.

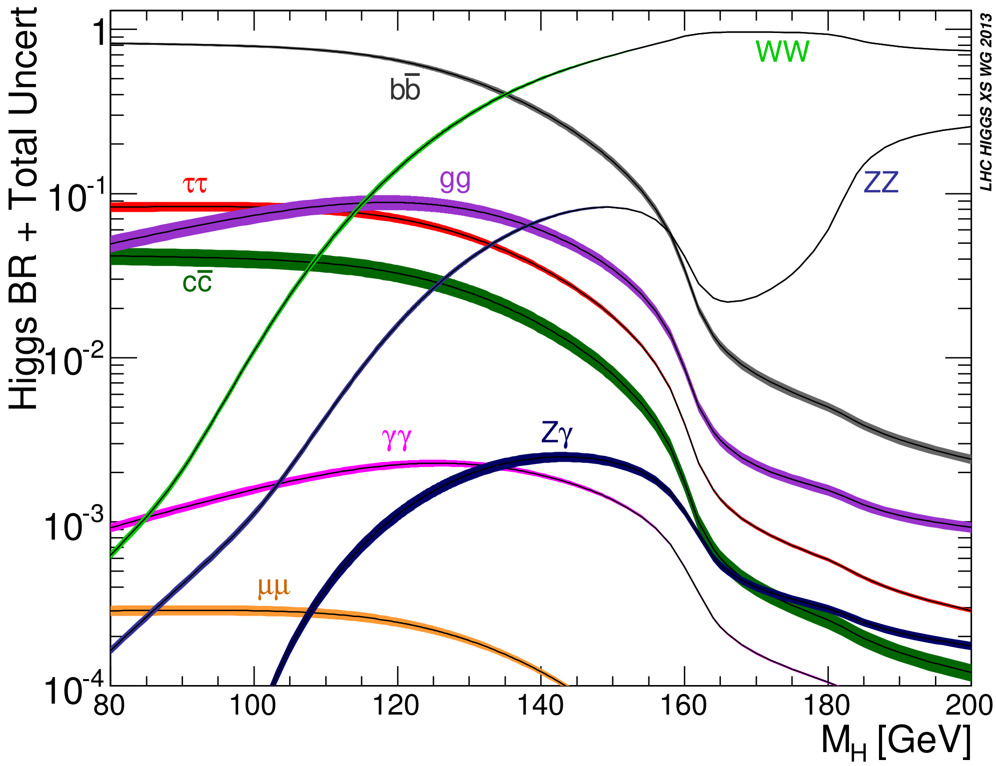


**Figure 1.6:** Higgs boson decay channels. At 125 GeV the dominant decay mode is $H \rightarrow b\bar{b}$.

Even though the facts above tell us about how great the SM is, the SM is still far from being perfect. Masses of elementary particles are the parameters in this theory, they do not come from SM predictions. It is hypothesised that the SM could be a part of the larger ultimate theory, the so-called "The Theory of Everything" (TOE), which is to be written (had been a lifelong journey of another genius, Einstein [26]). There is hope that the TOE will be able to explain many phenomena, such as the quark mass hierarchy, flavor mixing, etc. Also, in the SM all neutrinos are massless, however, it has been shown that they have a non-zero mass [27]. This fact is one of the main motivations for theorists to look for extensions of the SM.

# Chapter 2

# Theory

In the previous chapter we introduced the SM and discussed particles and their interactions that are described by this theory. In this chapter we will discuss first the general mathematical formalism of the SM and in the second part we will focus on the double Higgs boson physics in the Beyond the Standard Model (BSM) theory.

## 2.1 Lagrangian formalism of the Standard Model

The SM uses the Lagrangian mechanics as the mathematical approach to describe quantitatively the interactions of elementary particles and fields. The SM Lagrangian can be split into four main contributions [28]:

$$\mathcal{L}_{SM} = \mathcal{L}_{YM} + \mathcal{L}_{ferm} + \mathcal{L}_{H} + \mathcal{L}_{Yuk} \tag{2.1}$$

where

- $\mathcal{L}_{YM}$ represents gause bosons and their self-interactions,
- $\mathcal{L}_{ferm}$ describes fermions and their interactions with the gauge bosons,

- $\mathcal{L}_H$ characterises Higgs boson, its self-interaction, and interaction with the gauge bosons to give them mass,
- $\mathcal{L}_{Yuk}$ gives details of fermions and their interactions with the Higgs boson, which through the Yukawa mechanism give mass to fermions.

The first term in the SM Lagrangian in full can be written as:

$$\mathcal{L}_{YM} = -\frac{1}{4}W^i_{\mu\nu}(x)W^{\mu\nu}_i(x) - \frac{1}{4}B_{\mu\nu}(x)B^{\mu\nu}(x) - \frac{1}{4}G^a_{\mu\nu}(x)G^{\mu\nu}_a(x) \tag{2.2}$$

where

$$B_{\mu\nu}(x) \equiv \partial_\mu B_\nu - \partial_\nu B_\mu \tag{2.3}$$

$$W^i_{\mu\nu}(x) \equiv \partial_\mu W^i_\nu(x) - \partial_\nu W^i_\mu(x) - g\varepsilon^{ijk}W^j_\mu W^k_\nu \tag{2.4}$$

$$G^a_{\mu\nu}(x) \equiv \partial_\mu G^a_\nu(x) - \partial_\nu G^a_\mu(x) - g_s f^{abc}G^b_\mu G^c_\nu \tag{2.5}$$

with $\mu$ and $\nu$ indices running from 0 to 3, SU(2) indexes $i, j, k = 1, 2, 3$, SU(3) indices given by $a, b, c = 1, ..., 8$, and $\partial_\mu$ and $\partial_\nu$ represent four-vector covariant derivatives. According to the Noether's theorem, each symmetry is intrinsically connected to the conservation law [29]. The fields in the $\mathcal{L}_{YM}$ are connected to their corresponding underlying symmetries in the following way:

- $B_{\mu\nu}$ corresponds to $U(1)$ symmetry of the weak hypercharge $Y_k$ with U(1) being a unitary one-by-one matrix (a scalar),
- $W^i_{\mu\nu}$ corresponds to $SU(2)_I$ symmetry of the weak isospin $I^i_w$. Another common representation is $SU(2)_L$, since only left-handed SM fermions are transformed

under this symmetry. $SU(2)_L$ is a unitary two-by-two matrix with the determinant equal to one.

- $G^a_{\mu\nu}$ corresponds to $SU(3)_c$ symmetry of the QCD color charge with $SU(3)_c$ being a unitary three-by-three matrix with the determinant equal to one.

The "B" field is a kinematic term, "W" and "G" terms describe interactions among the bosons, $g$ and $\varepsilon$ are $SU(2)_L$ coupling and structure constants, $g_s$ and $f$ are coupling and structure constants for $SU(3)_c$.

The second term in the SM Lagrangian shows how fermions interact with the gauge bosons. Notice, that the mass terms are still absent:

$$\mathcal{L}_{ferm} = i\bar{\Psi}_L \not{D}\Psi_L + i\bar{\psi}_{l_R}\not{D}\psi_{l_R} + i\bar{\Psi}_Q\not{D}\Psi_Q + i\bar{\psi}_{u_R}\not{D}\psi_{u_R} + i\bar{\psi}_{d_R}\not{D}\psi_{d_R} \tag{2.6}$$

In the Eq. 2.6, $\Psi$ represents a doublet of a charged lepton and a corresponding neutral lepton within the same lepton family of $SU(2)_L$, the subindex Q is reserved for a family of quarks, and $\psi_R$ describes a right-handed leptonic singlet. Gauge boson interactions are present due to the derivative term:

$$D_\mu = \partial_\mu + igI^i_w W^i_\mu + ig'Y_w B_\mu + ig_s T^a_c G^a_\mu \tag{2.7}$$

Physical fields in this notation are represented by a linear combination of W and B fields:

$$\begin{aligned} A_\mu =& B_\mu \cos\theta_W + W^3_\mu \sin\theta_W \\ Z_\mu =& -B_\mu \sin\theta_W + W^3_\mu \cos\theta_W \end{aligned} \tag{2.8}$$

where $\theta_W$ is known as the *Weinberg angle* [30].

With the first two terms of the SM Lagrangian one obtains a valid theory of fermions and bosons, however, these particles are massless in this theory [31], which evidently contradicts the reality. To solve this issue and to ensure that weak bosons are massive, one has to introduce a Higgs field. Higgs mechanism enters the SM Lagrangian through the corresponding Higgs Lagrangian term given by

$$\mathcal{L}_H = (D_\mu\Phi)^\dagger(D^\mu\Phi) - V(\Phi), \qquad V(\Phi) = -\mu^2(\Phi^\dagger\Phi) + \frac{\lambda}{4}(\Phi^\dagger\Phi)^2 \tag{2.9}$$

where

$$\Phi = \begin{pmatrix} \phi^+ \\ \phi^0 = (v + H + i\chi)/\sqrt{2} \end{pmatrix} \quad \text{with} \quad v = 2\sqrt{\frac{\mu^2}{\lambda}} \tag{2.10}$$

here $\mu$ and $\lambda$ are parameters of the Higgs potential. The Higgs field vacuum expectation value (*vev*) $v$, after the SSB, can be expressed in terms of $\mu$ and $\lambda$. See Fig. 2.1 for the Higgs potential before and after the SSB. The importance of the $\mathcal{L}_H$ in the SM Lagrangian is crucial: after rearranging terms the bosons finally have masses given by:

$$M_W = \frac{gv}{2}, \quad M_Z = \frac{M_W}{\cos\theta_W}, \quad M_H = \sqrt{2\mu^2} \tag{2.11}$$

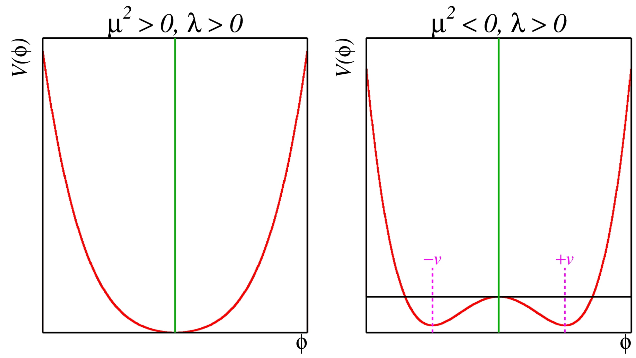


**Figure 2.1:** Shape of the Higgs potential before and after the SSB that is determined at the leading orders by $\mu$ and $\lambda$ parameters [32].

The final contribution to the SM Lagrangian is the Yukawa term, with Yukawa Lagrangian given by:

$$\mathcal{L}_{Yuk} = -i\bar{\Psi}_L G_l \psi_{l_R} \Phi - i\bar{\Psi}_Q G_u \psi_{u_R} \tilde{\Phi} - i\bar{\Psi}_Q G_d \psi_{d_R} \Phi + h.c. \tag{2.12}$$

where $\tilde{\Phi} = i\sigma^2\Phi^*$. The masses of fermions enter the equations through the $3 \times 3$ matrices G, which are free parameters in the SM and have to be determined from the experiment. The mass of each fermion is proportional to the Yukawa coupling of the corresponding fermion to the Higgs boson, see Fig. 1.4.

The Higgs boson mass is proportional to the $\mu$ parameter. In 2012, with precise single Higgs boson mass measurements from both ATLAS and CMS experiments, the value of $\mu$ was determined. Since that time many analyses at CERN have been targeting the measurement of the $\lambda$ parameter, because it is related to the shape of Higgs potential. In the SM having the "Mexican hat" Higgs potential, the simplest potential characterised by $\mu$ and $\lambda$ parameters, is sufficient to obtain the SSB phenomenon. This gives mass to fermions and bosons. However, the shape of the Higgs potential may be different and direct precise determination of the $\mu$ and $\lambda$ parameters is a sensitive tool to test the limitations of the SM and may open doors to the BSM effects. The simplest interaction that is probing the Higgs potential directly is the one where two Higgs bosons (HH) are present. All this makes HH physics, the topic of this thesis, one of the main goals for the future High Luminosity LHC (HL-LHC).

IN THE INTRO??While the mass parameter has been measured fairly accurately, $\lambda$ parameter requires even HL-LHC to run for many years to get enough statistics since HH processes are rare and are of almost three orders of magnitude lower rate than the single Higgs boson production. Technically, the amount of the HL-LHC data is not enough to reach the sensitivity of the SM for HH processes. At the same time, several BSM models predict resonant HH production to which even the current LHC data could be sensitive. In this theories, HH is produced through the decay of a heavy narrow width resonance, which is not a part of the SM. Thus, if such processes are found, this will open a new chapter in the HEP physics. In this thesis we focus on the resonant production of the HH system, which further decays to leptons and quarks. With the available CMS data, resonant HH analyses are starting to approach the needed sensitivity to rule out some BSM theories and test further the most promising ones.

## 2.2 Double Higgs in Beyond the Standard Model

Several BSM theories [33–35] predict a resonant production of the double Higgs boson events through a heavy resonance of a narrow width ($\sim O(1-10)$ GeV) [36]. In this dissertation data is compared with respect to predictions from the Warped Extra Dimensions theory (WED) [37]. WED theory addresses the hierarchy problem by adding additional fifth dimension to the 4-dimensional (4D) space-time. In the framework that Randall and Sundrum (RS) [38] introduced, 4D space is an EFT approximation of the higher dimensional space. The extra dimension exists between the gravity (Planck) and weak (TeV) flat 4D branes 2.2 and is called the "bulk". The bulk is described by the exponentially decaying metric.

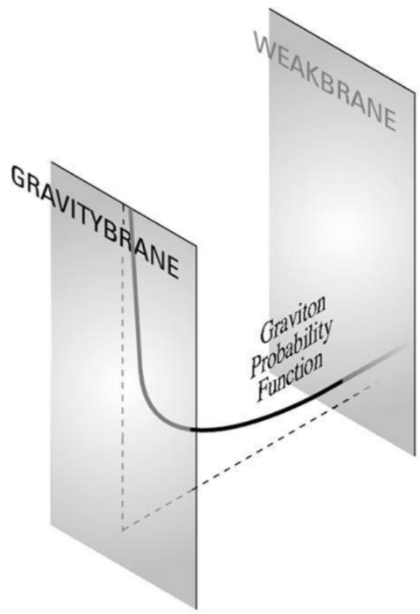


**Figure 2.2:** 5D space in the RS model [39].

The free parameters of the RS model are the brane separation factor $k$ and the size of the compactified dimension $r_c$. The curvature factor is given by $k \approx \sqrt{\frac{\Lambda}{M_5^2}}$, where $\Lambda$ is the ultraviolet cutoff of the theory and $M_5$ is the 5D Planck mass. The radius of the extra dimension $r_c$ is proportional to the parameter $1/k$ and the logarithm of $1/vev$. The hierarchy between the Planck scale and the electroweak scale is reproduced for $k \cdot r_c \approx 11$. In this case the RS model matches the observations of the Higgs boson being closer to the TeV brane and fermions having light mass (located near the Planck brane).

Since LHC had provided us with no evidence of the SM particles interacting with the RS particles, the RS model considered in this thesis hypothesises that SM particles are confined to branes. Another reason could be due to the fact that Kaluza-Klein

(KK) [40] partners of the SM particles are too massive to be produced at the LHC, but this scenario is not addressed in this dissertation. In the RS model under study two new particles appear. When the bulk is compactified, the WED theory predicts the existence of the KK excitations of the gravitational field, with the zero-th KK mode being a graviton, the mediator of the gravitational force. The graviton (spin 2) is the first WED particle predicted by the RS model. The graviton can propagate freely in the full higher-dimensional space of the 5D bulk. The other RS particle is a radion (spin 0). Its existence is required to stabilise the size of the extra dimension.

The theoretical arguments put forward by the authors [41] suggest the RS parameters $k$ and $\bar{M}_{Pl}$ to be constrained by the following range of values: $0.01 \leq k/\bar{M}_{Pl} \leq 1$. The parameter $k$ is of the order of the Planck scale and $\bar{M}_{Pl} = \sqrt{\frac{M_5^3}{k} \cdot (1 - e^{-2\pi k r_c})}$ is a reduced 4D $M_{Pl}$. Considered in this measurement graviton and radion are RS particles with a KK state mass of the order of TeV.

Let us denote a part of the KK 5D wave function, often called a profile, as $f_X^{(n)}(\phi)$, where n is referred to the n$^{th}$ KK mode. Then the graviton can be decomposed as $\sum_{n=0}^{\infty} h_{\mu\nu}^{(n)}(x_\mu) \cdot f_X^{(n)}(\phi)$. Its zero-th mode corresponds to the massless graviton and the first mode corresponds to the lightest KK graviton (later graviton) which has the effective mass of the O(TeV). The profiles for all the matter fields are described by a combination of Bessel and exponential functions. The Lagrangian describing the interaction of the graviton with the SM fields is given then by

$$\mathcal{L}_{graviton} = -\frac{x_1 \tilde{k}}{m_G} h^{\mu\nu(1)} \times d_i T_{\mu\nu}^{(i)}, \tag{2.13}$$

where $x_1 = 3.83$ is the first zero of the Bessel function for a given profile, $\tilde{k} = k/\bar{M}_{Pl}$, $h^{\mu\nu}$ is a symmetric tensor, $m_G$ is the effective mass of the graviton of the order of TeV, $d_i$ is an integral of the profiles of the SM fields and KK graviton, and $T_{\mu\nu}^{(i)}$ is a

4D canonical energy-momentum tensor [42] for any SM field $i$. A free parameter $\tilde{k}$ varies from 0.01 to 1 when $m_G$ is varied from 100 to 1500 GeV.

For radion the Lagrandian is given by:

$$\mathcal{L}_{radion} = -\frac{r}{\Lambda_R} \times a_i T_{\mu}^{\mu(i)}, \tag{2.14}$$

where $r$ is a 5D radion field, $\Lambda_R$ is the scale parameter proportional to $k \cdot \sqrt{(\frac{M_5}{k})^3}$, and $a_i$ is the coupling of the radion to the SM field $i$. In the studied RS model the profiles of the graviton and radion arise naturally as being localised at the TeV brane for the coupling of a radion and a graviton to the massive SM fields to be of the order of 1.

In the SM the HH system is produced predominantly via two diagrams shown on Fig.2.3: the "box" and the "triangular" diagrams. They interfere destructively and the total cross section is thus lowered (Fig. 2.5 on the right). The box diagram dominates the double Higgs boson production and peaks near 400 GeV, as shown by the study performed by theorists, see [43]. In this measurement, though, the gravitons and radions in the search are expected to be produced by the BSM "contact interaction" Feynman diagram allowed by the WED scenario. These process is shown on Fig. 2.4. A graviton and a radion subsequent decays to HH system are thoroughly studied and the experimental results are compared to the theoretical predictions calculated for the WED model with the parameters $\tilde{k} = 0.1$ and $\Lambda_R = 3$ TeV.

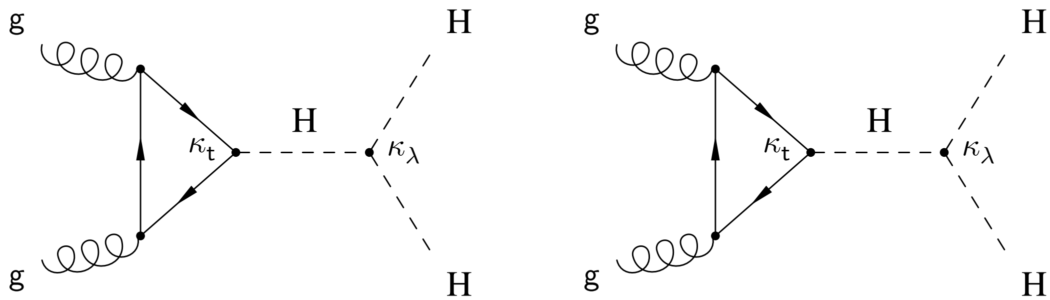


**Figure 2.3:** SM double Higgs boson production.

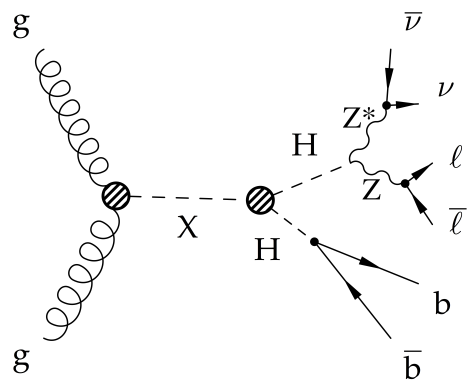


**Figure 2.4:** BSM Resonant double Higgs decay in the 2 b, 2 lepton, and 2 neutrino final state.

The kinematic distribution of the double Higgs mass remains to a high degree unchanged between 13-14 and 100 TeV (see Fig. 2.5 on the left), therefore, we can compare 100 TeV results produced by theorist to those analysed in this thesis that use the data delivered by the current 13 TeV LHC machine. Fig. 2.5 refers to the box and the triangular diagrams as "box" and "tri", and to the non-linear interaction as "nl" [44].

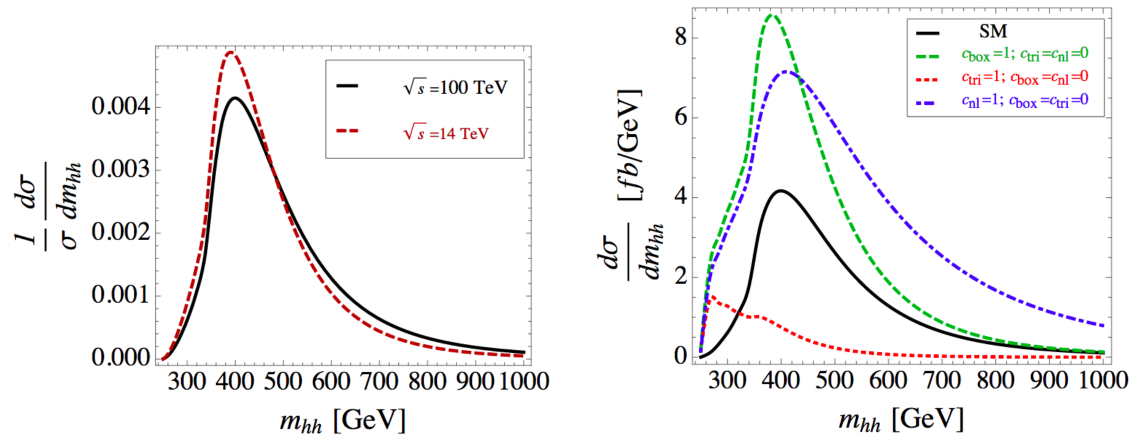


**Figure 2.5:** Left: comparison of the double Higgs boson mass distribution at the LO at $\sqrt{14}$ and $\sqrt{100}$ TeV center-of-mass energy. Right: the total SM HH cross section and the individual contributions [44].

This thesis separately addresses resonant graviton and radion decays into two SM Higgs bosons with the subsequent decays of one Higgs boson to a pair of b quarks, and the other Higgs boson to W or Z boson pairs. W bosons are allowed to decay only leptonically. For Z boson decays, the signature is characterised by the on-shell Z boson decaying into a pair of charged leptons and the off-shell Z boson decaying to neutrinos (see Fig. 2.4). The final state that this thesis focuses on consists of two b quarks, two charged leptons, and two neutrinos. This signature has a branching fraction of approximately 2.8%.

To finish this chapter, it is instructive to show all the decay channels of the double Higgs system to the SM particles, which is summarised in the Fig. 2.6. Both the horizontal and the vertical axes show decays of a single Higgs boson to two SM particles. In this representation, each square on the plot specifies a branching fraction of one of the double Higgs boson decays, with the probability of the decay given by the colour field on the right.

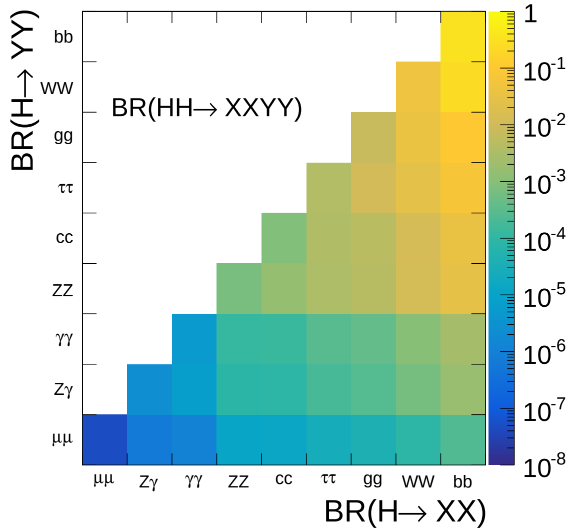


**Figure 2.6:** Double Higgs decay channels. The SM branching fractions are represented by the colour palette.

Chapter *3*

# LHC and the CMS experiment

CERN accelerator complex is a sequence of machines that produces and accelerates "bunches" of $10^{11}$ protons to nearly the speed of light. In the Large Hadron Collider (LHC) the bunches collide at specific interaction points (IP), where the four main experiments are located: ALICE, ATLAS, CMS, and LHCb. We will start this section with the discussion of the LHC machine and then describe the CMS detector.

## 3.1 The Large Hadron Collider

### 3.1.1 The history of the LHC

The story of the LHC begins in 1977, when the CERN director general Sir John Adams suggested that the tunnel of the Large Electron-Positron Collider (LEP) can be reused to accommodate the future hadron collider of more than 3 TeV energies **??**. At the 1984 ECFA-CERN workshop on a "Large Hadron Collider in the LEP Tunnel" **??**, the physics goals of the LHC were stated: confirmation of the BEH mechanism, search for the Higgs Boson, and exploration of the origin of masses of W and Z bosons. The parameters of the proposed LHC were very ambitious: the centre-of-mass (COM) collision energy of 10 to 20 TeV, and a target instantaneous luminosity of $10^{33-34}\frac{1}{cm^2 s}$.

Large Hadron Collider (LHC) is the most powerful particle accelerator that has ever been built. It is located at the border of France and Switzerland at a depth from 50 to 175 m underground. LHC ring is 26.7 km in circumference and it is the final stage in a sequence of accelerators.

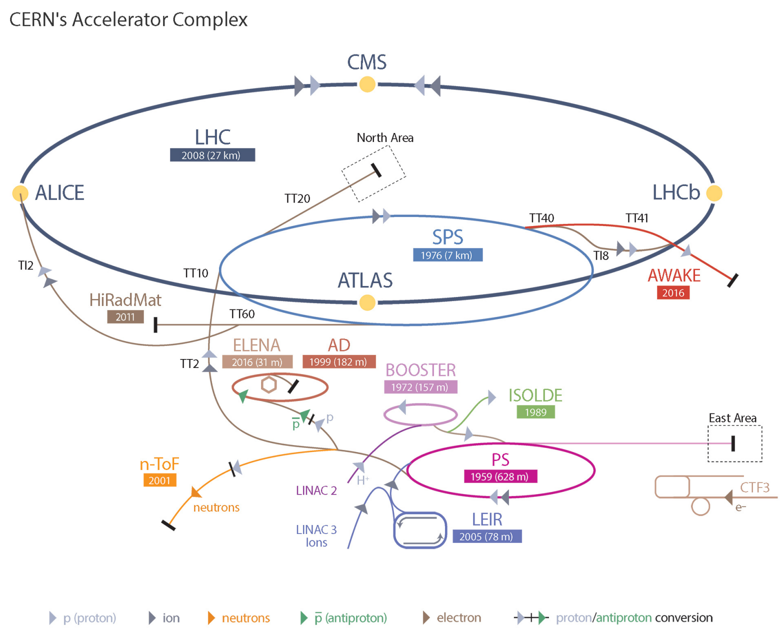


**Figure 3.1:** Schematic layout of the LHC.

It is a complex process to start proton-proton collision in the LHC at 13 TeV and, therefore, the process consists of several stages (see Fig. 3.1). Everything begins with the bottle of hydrogen. The hydrogen atoms from the bottle are fed into the source chamber of the Linear Accelerator (Linac). In the chamber the hydrogen is heated up to the plasma state until electrons are stripped off of the hydrogen atoms. Then electrons are removed and remaining protons are directed to the first acceleration stage which increases the energy of protons to 50 MeV. After Linac, the beam of protons is injected into the Proton Synchrotron Booster (PSB). PSB contains four rings each accelerating a bunch of protons (a moving collection of protons of a narrow length) to 1.4 GeV. The third stage is the Proton Synchrotron (PS), which splits the incoming beam into 72 bunches separated by 7.5 m. The energy of the protons is increased to 25 GeV. After that, the protons are sent to the Super Proton Synchrotron (SPS), where they are accelerated to 450 GeV. SPS then fills the LHC ring with two beams each consisting of 2808 bunches of protons with nearly $10^{11}$ protons in total. It takes SPS about $O(10)$ minutes to fill each LHC ring with bunches. In the LHC two beams are circulating in opposite directions in two separate beam pipes. During standard data taking beams circulate for $O(10)$ hours.

### 3.1.2 LHC operations

The first LHC budget plan was finalised in 1996 and the final cost was approved just a few years later. The first proton beam entered the LHC ring in 2008. However, an incident intervened the LHC plans. It was caused by the mechanical damage of the tunnel equipment due to the release of the helium. Thus, the real data taking period (called LHC Run-1) had started only in 2010 and lasted for two years with 7-8 TeV COM energies. The recorded dataset contained enough Higgs bosons to claim a discovery of this rarely produced particle. After this achievement, the LHC was closed for the first long shutdown (LS1) that happened in 2012. During this time necessary upgrades of the main detectors and the LHC were performed. This was an unavoidable and essential step to prepare the LHC for more challenging environment of COM energies increased to 13 TeV.

If we denote the area of $10^{-28}\ m^2$ as barn (b), then in terms of these new units the LHC can theoretically produce $80 - 120/fb$ of data a year. In practice numbers were lower, because LHC operated at the revolution frequency below the nominal, used fewer proton bunches in the beam, etc. All this resulted in lower than expected instantaneous luminosity, which is a very important term in collider physics and will be explained in the next section.

The LHC Run-2 has started in 2015 and the CMS collected 4.2 $fb^{-1}$ of data that year. Over the course of the 2016 data taking, an integrated luminosity of 35.9 $fb^{-1}$ was recorded. This luminosity is the amount of data that has been collected by the CMS detector and later approved by the CMS physics coordination for the use in the physics analyses. The data set of proton-proton collisions collected in 2016 at 13 TeV COM energy is used in this thesis to analyse double Higgs boson decays. Together with the 2017 and 2018 data taking, almost 150 $fb^{-1}$ have been delivered and recorded by the CMS detector during the whole Run-2 period of four years.

At the moment of writing this thesis, the LHC has entered the LS2. The next data taking will resume in 2020 and proton-proton collisions will continue for three years with the expected delivered integrated luminosity equal to nearly 300 $fb^{-1}$. This will conclude the LHC Phase-1 programme.

The new upgraded LHC, the High-Luminosity LHC (LHC) or the Phase-2, will start operations in 2026 and run until 2035. The COM energy will be increased to 14 TeV and one expects to record an unprecedented dataset of 3000 $fb^{-1}$.

### 3.1.3 Luminocity

The instantaneous luminosity is the coefficient which relates the cross section $\sigma$ of the process to the number of events $N_{events}$ produced during the interaction: $N_{events} = \mathcal{L}\sigma$. Luminosity is the parameter controlled by the machine and can be written as:

$\mathcal{L} = \frac{N^2 n_b f_{rev}}{4\pi\sigma_x\sigma_y}$

where $N_b$ is the number of particle in the colliding bunch, $n_b$ is the number of colliding bunches in the beam, $f_{rev}$ is the revolution frequency of the beam, $\sigma_x$ and $\sigma_y$ are the standard deviations of the beam density profile (BDP) in the transverse plane, where it is assumed that the BDP of both beams can be described by a Gaussian distribution.

To maximise the amount of collected data, the luminosity parameter should be as high as possible. It is worth noting that the luminosity is not constant and decays with time due to the degradation of the initial circulating beams. Theoretical decay time (the time to reach $1/e$ level) is approximately 29 h. In practice, taking into account the decrease of protons in the bunch due to collisions, contributions from the intrabeam scattering, scattering on the residual gas, etc., the real luminosity lifetime is about 15 h.

A useful variation of the luminosity parameter is a total integrated luminosity. This is the number normally quoted for the dataset collected over the period T:

$L = \int_0^T \mathcal{L} dt.$

In collider physics the "beam dump" is a process of burning off exhausted low luminosity beams by intentionally directing them towards the target made of concrete and steel. The time from the start of the collisions to the beam dump is usually called the "run".

We can calculate the amount of data delivered by the LHC during a single run period $O(10)$ h. Performing the integration, we obtain:

$L = \mathcal{L}_0 \tau_{\mathcal{L}} \left[ 1 - e^{\frac{-\tau_{run}}{\tau_{\mathcal{L}}}} \right],$

where $\mathcal{L}_0$ is the initial peak instantaneous luminosity at the start of the run, $\tau_{run}$ is the total duration of a run, and $\tau_{\mathcal{L}}$ is the luminosity lifetime. The optimum run time is 12 hours. During the runs, the LHC centre needs to dump the old beams, fill the rings with the new beams, and increase ("ramp") the energy of new beams to 13 TeV. After that a new run can be started. This restarting process normally takes two to six hours.

### 3.1.4 LHC infrastructure

The equipment of the LHC tunnel serves several purposes with the main objective to keep the colliding beams on the circular orbit. This requires a complex synchronised work of bending dipole magnets, cooling systems, accelerating radio frequency cavities, and vacuum insulation systems.

#### 3.1.4.1 Magnets

Most of the LHC circumference is used by 1232 superconducting magnets placed evenly around the tunnel to approximate the circular orbit. These are dipole magnets (see Fig. 3.2) that bend the beam and keep it on the circular orbit, that is why they are commonly called "Main Bends" (MB). The proven technology existed since Tevatron and relied on NbTi superconductors. This technology also satisfied the LHC cost and performance requirements, thus, it was decided to reuse the same choice of the alloy for the LHC superconducting dipole magnets that steer the proton beams.

The dipoles need to produce the magnetic field of 8.3T. Each dipole is 16.5 $m$ (with ancillaries) long and 570 $mm$ in diameter and is placed inside of the dipole cryostat which is called the "Helium bath".

This cryostat is a long cylindrical tube 914 $mm$ in diameter made of low-carbon steel, where the dipole mass is cooled down to 1.9 $K$. Even though the inner structure of such cryostat is very complex and includes two beam pipes, two sets of coils for two beam pipes, vacuum pipes etc., one normally calls this compound object simply a dipole magnet. The name "dipole" is reserved for MBs since for each beam pipe the magnet consist of two "poles" that provide a vertical magnetic field similarly to a simple dipole system of magnets.

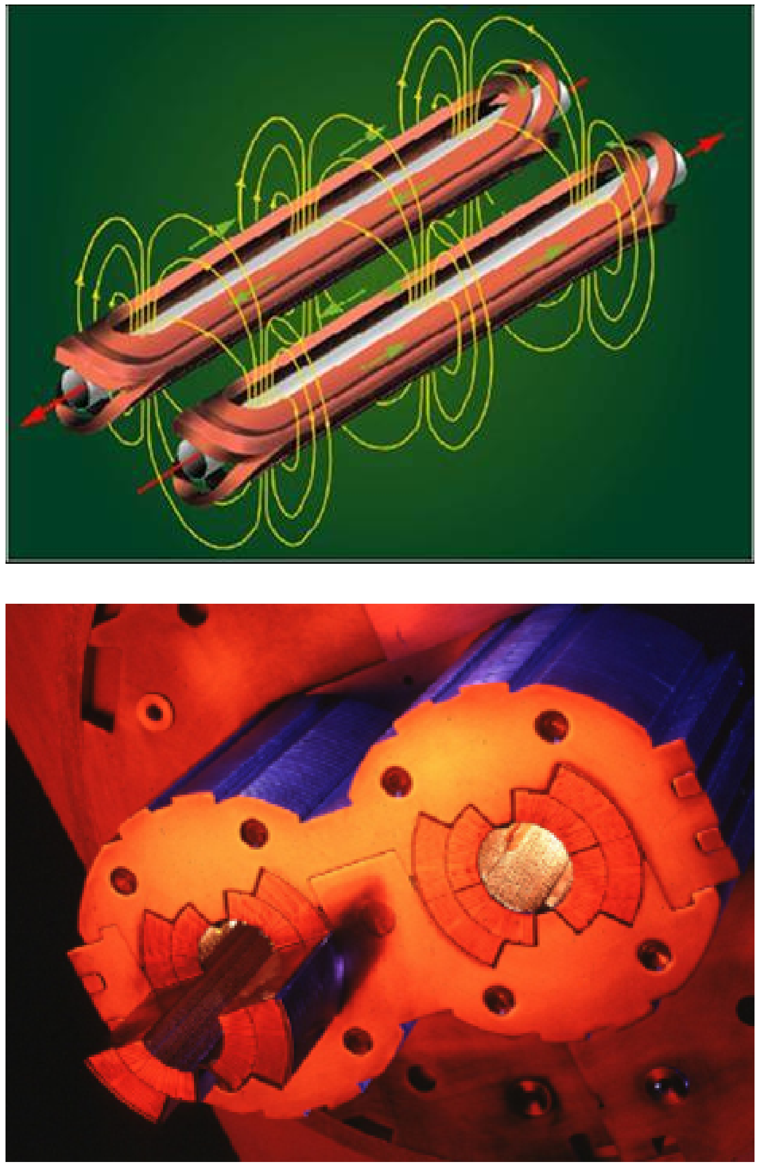

**Figure 3.2:** LHC dipole magnets. Top: two dipole coils and magnetic field lines. Bottom: two beam pipes with the coils inside of the dipole magnet.

A dipole magnet must be curved to help a chain of dipoles complete 360 degrees. The curvature is 5.1 *mrad* per dipole, which is equivalent to a sagitta of about 9 mm, corresponding to a radius of curvature of 2812.36 m.

The other important set of magnets is quadrupoles. They are used to ensure the proper beam dynamics. In total 392 quadrupole magnets ranging from 5 to 7 metres in length are used to squeeze the beam in transverse direction and to keep it narrow during the run duration. Additional special quadrupole magnets (SQM) are installed right before the IPs to focus the beams even more. That increases the density of protons in the beam and guarantees the maximum luminosity. In addition, SQMs help to decrease the chance of the parasitic collisions when bunches from the same beam or bunches outside of the IP centre interact (see Fig. 3.3). To further correct the beam path (orbit), about 5000 higher order correcting magnets are used, which are evenly spaced around the circular trajectory of the LHC.

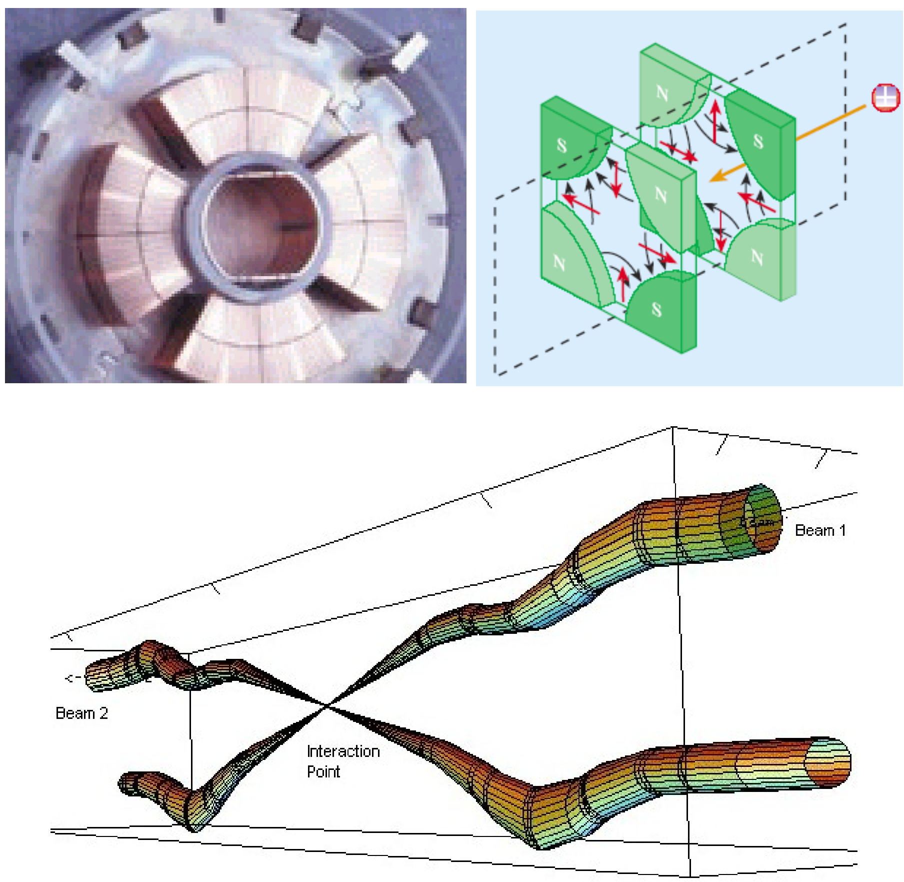


**Figure 3.3:** LHC quadrupoles. Top left: the coil of the quadrupole magnet. Top right: schematic view of the magnetic fields in the quadrupole. Bottom: two beams and the IP.

To power the LHC, 1612 electrical circuits are used. Mostly these circuits are needed to power the dipole and quadrupole magnets, which is done in eight evenly spaced location of the LHC. A total of 3286 current leads are needed to connect all the circuits and power cables. More than a thousand of the leads operate between 600 A and 13 kA (see Fig. 3.4). The other leads work in the range 60 to 120 A.

**Figure 3.4:** 13 kA high-temperature superconducting current lead.

#### 3.1.4.2 Cooling System

To ensure that dipoles are in the superconducting state, they have to be cooled to 1.9 K using superfluid helium-4.

The cooling (cryogen) system is needed to keep superconducting LHC magnets at the appropriate temperature. The choice of the cooling gas depends on the magnet type and location. This dictates the required range of temperatures, which differs from system to system by 75 K. The cryogen system uses layered design with the temperature becoming progressively colder going from outside the dipoles closer to the beam pipe.

The "coldest" part of the cryogen system is designed for the inner part of the dipoles. This system (see Fig. 3.5) must cool down 37 Mkg of the LHC magnets within 15 days to the required temperatures, which is done through the system of pipes that transport the flow of the superfluid helium. The cryogen system must also be able to deal with the fast increases of the pressure flow and flow surges, as it is crucial for the LHC operation to keep dipoles constantly cooled and at the superconducting state.

The LHC tunnel is inclined in the horizontal plane by 1.41°. This translates to 120 m difference in the vertical location of two diametrically opposite points of the tunnel with respect to the surface level and results in the additional hydrostatic pressure that can affect the flow of helium. This has been an important concern during the design of the cryogen system.

Since the cost to cool the LHC parts to 1.8-1.9 K temperatures is high, several temperature levels are employed (see Fig. 3.5):

- 50 to 75 K for the thermal shielding used in the dipoles,
- 20 to 300 K for upper ("warm") sections of the high-temperature superconducting current leads,
- 4.6 to 20 K for lower temperature interception,
- 4.5 K for radio frequency cavities and lower ("cold") sections of the high-temperature superconducting current leads,
- 4 K for the transportation system that directs the 1.8 K helium to dipoles,
- 1.9 K for helium in the superfluid state to cool magnet masses.

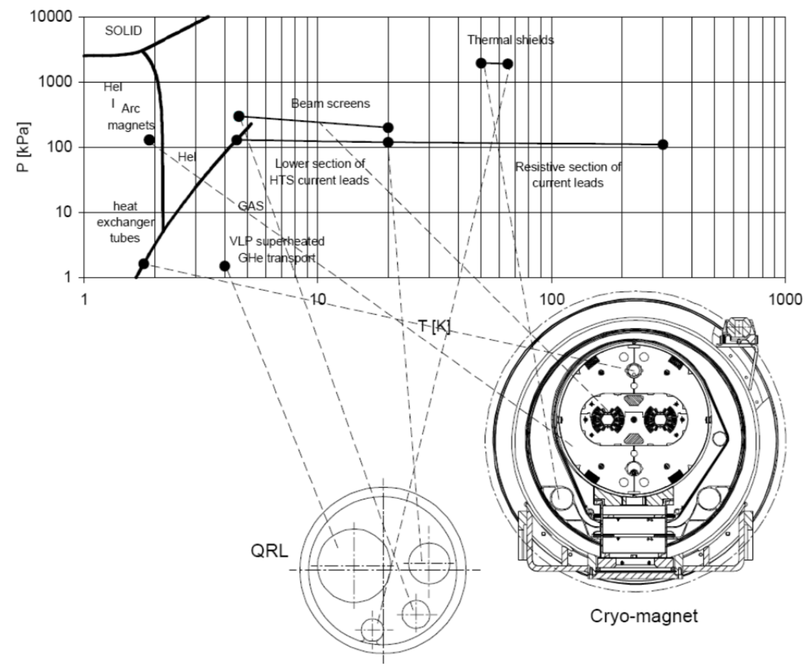


**Figure 3.5:** LHC cryogenic states and the temperature scale.

#### 3.1.4.3 Radio Frequency Cavities

Proton bunches need to be ramped to 7.5 TeV energies. To achieve this 13 TeV COM energy, eight superconducting radio-frequency cavities (RFC) are used per beam. They are located in front of the IPs of four experiments. Electromagnetic waves of 400 MHz with a peak field strength of 5.5 MV/m adjust the speed of protons in bunches. Each RFC (see Fig. 3.6) increases the energy of protons by 60 keV per revolution and it takes $O(20)$ minutes to reach 6.5 TeV beam energy. The RFC frequencies are increased gradually by 1 kHz to match the speed up of protons in the bunch as they gain more energy. When the ramp is completed, the RFCs are used to compensate for small energy losses due to the synchrotron radiation (7 keV per revolution).

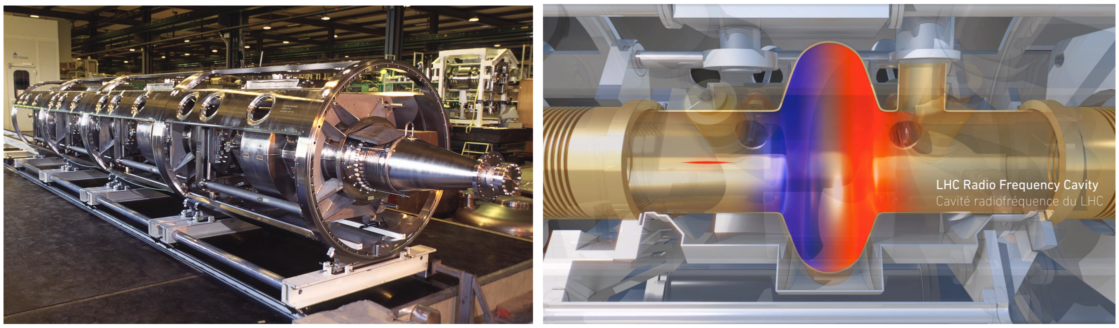


**Figure 3.6:** LHC RF cavities. Left: a cryomodule with four RF cavities. Right: a schematic drawing of a single RF cavity. The colour field is used to denote Positive (red) and Negative (blue) polarities. A narrow beam traversing the cavity is shown in red.

#### 3.1.4.4 Vacuum System

The work of the LHC depends on three vacuum systems [**?**]. Without them, dipoles will not be at the superfluid state, the beams will not be able to circulate, and no stable collisions would be taken. With a total of 104 kilometres of vacuum pipes, the LHC owns the largest vacuum system in the world. The main types of vacuum systems are:

- insulation vacuum for cryomagnets,
- insulation vacuum for the helium distribution line,
- beam vacuum.

The insulation vacuum is needed to ensure the operations at both low temperatures of the magnets and the room temperatures in the tunnel. The insulation vacuum of $10^{-6}$ mbar is used for a total of 15000 cubic metres. To build this vacuum system, the LHC used 250,000 welded joints and 18,000 vacuum seals.

The vacuum for the helium distribution lines is needed to protect from the heat the flow of the helium-4. This helium flow is used to cool down the dipole mass.

Cryogenic distribution lines (QRL) of 3.3 km each are connected to eight cryogenic plants that pump the helium-4 into the LHC. The vacuum in these systems is at $10^{-7} - 10^{-10}$ mbar level.

For the beam pipes the LHC uses ultra-high vacuum of $10^{-10}$ mbar at cryogenic temperature of 5 K with the vacuum getting progressively closer to $10^{-11}$ mbar near the IPs, because in these locations collisions take place and any additional gas is highly undesirable. This vacuum is the emptiest space in the Solar System. This ultra-high vacuum is needed to reduce the beam degradation due to the beam-gas interactions in the pipe and parasitic collisions of bunches with the collimators near the IPs.

Vacuum system are affected by the heat produced from the synchrotron radiation emitted by the proton beams when they are bent. To reduce the amount of this heat and to narrow down the beam size in the transverse direction when the beam widens, the LHC uses "beam screens", which operate between 5 and 20 K.

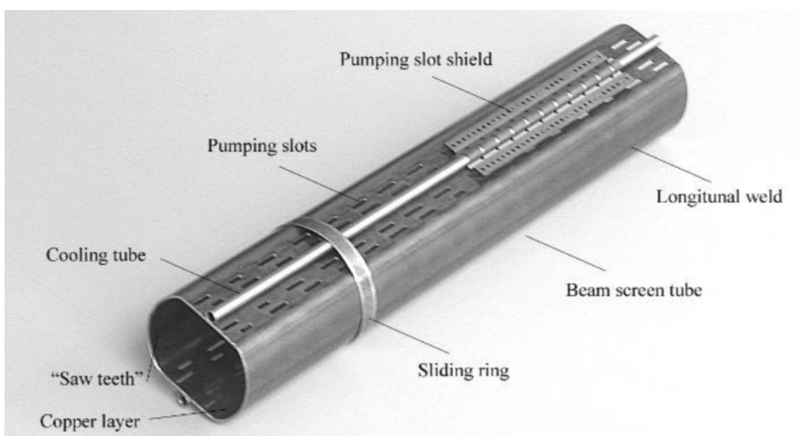


**Figure 3.7:** Beam screen.

The beam screens are necessary to reduce the number of protons scattering on the residual gas of the beam pipes, which could lead to a magnet quench and even interrupt the machine operation. The table below summarises the main heat sources that degrade the vacuum quality in the beam pipe, where the vacuum must exist at 1.9 K:

- synchrotron radiation (0.2 $W/m$ per beam),
- energy loss by nuclear scattering (30 $mW/m$ per beam),
- image currents (0.2 $W/m$ per beam),
- electron cloud related effects (vary).

Now, that we discussed the LHC collider, we can continue with one of the main LHC detectors - the CMS detector - the one that was used to collect the data analysed in this thesis.

## References

[1] Erwin Schrödinger. *Statistical thermodynamics; 2nd ed.* Cambridge Univ. Press, Cambridge, 1952.

[2] Richard Phillips Feynman, Robert Benjamin Leighton, and Matthew Sands. *The Feynman lectures on physics; New millennium ed.* Basic Books, New York, NY, 2010. Originally published 1963-1965.

[3] David J Griffiths. *Introduction to elementary particles; 2nd rev. version.* Physics textbook. Wiley, New York, NY, 2008.

[4] E A Davis and Isabel Falconer. *J.J. Thompson and the discovery of the electron.* Taylor and Francis, Hoboken, NJ, 2002.

[5] Oreste Piccioni. *The Discovery of the Muon*, pages 143–162. Springer US, Boston, MA, 1996.

[6] Carl Bender. Mathematical physics.

[7] G. Danby, J-M. Gaillard, K. Goulianos, L. M. Lederman, N. Mistry, M. Schwartz, and J. Steinberger. Observation of high-energy neutrino reactions and the existence of two kinds of neutrinos. *Phys. Rev. Lett.*, 9:36–44, Jul 1962.

[8] M. L. Perl, G. S. Abrams, and et al Boyarski. Evidence for anomalous lepton production in $e^+ - e^-$ annihilation. *Phys. Rev. Lett.*, 35:1489–1492, Dec 1975.

[9] K. Kodama et al. Observation of tau neutrino interactions. *Phys. Lett.*, B504:218–224, 2001.

[10] Eric W. Weisstein. Fundamental forces.

[11] S Chandrasekhar. *Newton's principia for the common reader*. Oxford Univ., Oxford, 2003. The book can be consulted by contacting: PH-AID: Wallet, Lionel.

[12] Hanoch Gutfreund and Jurgen Renn. *The road to relativity: the history and meaning of Einstein's "The foundation of general relativity" : featuring the original manuscript of Einstein's masterpiece*. Princeton University Press, Princeton, NJ, Apr 2015.

[13] J. Butterworth. *Smashing Physics*. Headline Publishing Group, 2014.

[14] W N Cottingham and D A Greenwood. *An Introduction to the Standard Model of Particle Physics; 2nd ed.* Cambridge Univ. Press, Cambridge, 2007.

[15] C. Patrignani et al. Review of Particle Physics. *Chin. Phys.*, C40(10):100001, 2016.

[16] Andrew Wayne. QED and the Men Who Made It: Dyson, Feynman, Schwinger, and Tomonaga by Silvan S. Schweber. *The British Journal for the Philosophy of Science*, 46(4):624–627, 1995.

[17] Michelangelo L Mangano. Introduction to QCD. (CERN-OPEN-2000-255), 1999.

[18] R. P. Feynman. The theory of positrons. *Phys. Rev.*, 76:749–759, Sep 1949.

[19] Matt Strassler. Of particular significance: Conversations about science with theoretical physicist matt strassler.

[20] S.L. Glashow. Partial symmetries of weak interactions. *Nucl.Phys.*, 22:579–588, 1961.

[21] F. Englert and R. Brout. Broken symmetry and the mass of gauge vector mesons. *Phys. Rev. Lett.*, 13:321–323, Aug 1964.

[22] Peter W. Higgs. Broken symmetries and the masses of gauge bosons. *Phys. Rev. Lett.*, 13:508–509, Oct 1964.

[23] G. S. Guralnik, C. R. Hagen, and T. W. B. Kibble. Global conservation laws and massless particles. *Phys. Rev. Lett.*, 13:585–587, Nov 1964.

[24] Pauline Gagnon. *Who cares about particle physics? : making sense of the Higgs boson, the Large Hadron Collider and CERN.* Oxford University Press, 2016.

[25] Precise determination of the mass of the Higgs boson and studies of the compatibility of its couplings with the standard model. Technical Report CMS-PAS-HIG-14-009, CERN, Geneva, 2014.

[26] Jennifer Ouellette. Einstein's quest for a unified theory. *APS*, 2015.

[27] S. M. Bilenky. Neutrino in Standard Model and beyond. *Phys. Part. Nucl.*, 46(4):475–496, 2015.

[28] Matthias U. Mozer. Electroweak Physics at the LHC. *Springer Tracts Mod. Phys.*, 267:1–115, 2016.

[29] Gennadi Sardanashvily. *Noether's theorems: applications in mechanics and field theory*. Atlantis studies in variational geometry. Springer, Paris, 2016.

[30] Steven Weinberg. The Making of the Standard Model. *Eur. Phys. J. C*, 34(hep-ph/0401010):5–13. 21 p. ; streaming video, 2003.

[31] Roger Wolf. *The Higgs Boson Discovery at the Large Hadron Collider*, volume 264. Springer, 2015.

[32] Jose Andres Monroy Montanez, Kenneth Bloom, and Aaron Dominguez. Search for production of a Higgs boson and a single Top quark in multilepton final states in pp collisions at $\sqrt{s} = 13$ TeV, Jul 2018. Presented 23 Jul 2018.

[33] Peisi Huang, Aniket Joglekar, Min Li, and Carlos E. M. Wagner. Corrections to Di-Higgs Production with Light Stops and Modified Higgs Couplings. 2017.

[34] Matthew J. Dolan, Christoph Englert, and Michael Spannowsky. New Physics in LHC Higgs boson pair production. *Phys. Rev.*, D87(5):055002, 2013.

[35] Shinya Kanemura, Kunio Kaneta, Naoki Machida, Shinya Odori, and Tetsuo Shindou. Single and double production of the Higgs boson at hadron and lepton colliders in minimal composite Higgs models. *Phys. Rev.*, D94(1):015028, 2016.

[36] Albert M Sirunyan et al. Search for Higgs boson pair production in the $\gamma\gamma\mathrm{b}\overline{\mathrm{b}}$ final state in pp collisions at $\sqrt{s} = 13$ TeV. 2018.

[37] Alexandra Oliveira. Gravity particles from Warped Extra Dimensions, predictions for LHC. 2014.

[38] Lisa Randall and Raman Sundrum. A Large mass hierarchy from a small extra dimension. *Phys. Rev. Lett.*, 83:3370–3373, 1999.

[39] Alexandra Oliveira. Gravity particles from Warped Extra Dimensions, predictions for LHC. 2014.

[40] Kunihito Uzawa, Yoshiyuki Morisawa, and Shinji Mukohyama. Excitation of Kaluza-Klein gravitational mode. *Phys. Rev.*, D62:064011, 2000.

[41] H. Davoudiasl, J. L. Hewett, and T. G. Rizzo. Phenomenology of the Randall-Sundrum Gauge Hierarchy Model. *Phys. Rev. Lett.*, 84:2080, 2000.

[42] Michael Forger and Hartmann Romer. Currents and the energy momentum tensor in classical field theory: A Fresh look at an old problem. *Annals Phys.*, 309:306–389, 2004.

[43] Chuan-Ren Chen and Ian Low. Double take on new physics in double Higgs boson production. *Phys. Rev.*, D90(1):013018, 2014.

[44] Roberto Contino, Margherita Ghezzi, Mauro Moretti, Giuliano Panico, Fulvio Piccinini, and Andrea Wulzer. Anomalous Couplings in Double Higgs Production. *JHEP*, 08:154, 2012.

[45]

[46] J. Alwall, R. Frederix, S. Frixione, V. Hirschi, F. Maltoni, O. Mattelaer, H. S. Shao, T. Stelzer, P. Torrielli, and M. Zaro. The automated computation of tree-level and next-to-leading order differential cross sections, and their matching to parton shower simulations. *JHEP*, 07:079, 2014.

[47] Thomas Junk. Confidence level computation for combining searches with small statistics. *Nucl.Instrum.Meth.*, A434:435, 1999.

[48] Glen Cowan, Kyle Cranmer, Eilam Gross, and Ofer Vitells. Asymptotic formulae for likelihood-based tests of new physics. *Eur. Phys. J.*, C71:1554, 2011. [Erratum: Eur. Phys. J.C73,2501(2013)].

[49] SM Higgs Combination. Technical Report CMS-PAS-HIG-11-011, CERN, Geneva, 2011.

[50] S. Frixione, P. Nason, and C. Oleari. Matching nlo qcd computations with parton shower simulations: the powheg method. *JHEP*, 11:070, 2007.

[51] S. Agostinelli et al. GEANT4—a simulation toolkit. *Nucl. Instrum. Meth. A*, 506:250, 2003.

[52] Gionata Luisoni, Paolo Nason, Carlo Oleari, and Francesco Tramontano. $HW^{\pm}$/HZ + 0 and 1 jet at NLO with the POWHEG BOX interfaced to GoSam and their merging within MiNLO. *JHEP*, 10:083, 2013.

[53] Comparison of nuisances for background only case, 350 GeV mass hypothesis. http://rkamalie.web.cern.ch/rkamalie/feb12/Comparison_of_nuisances_expectedSignal0_35

[54] Comparison of nuisances for s+b case, 350 GeV mass hypothesis. http://rkamalie.web.cern.ch/rkamalie/feb12/Comparison_of_nuisances_expectedSignal1_35

[55] k-factor for DY/Z. https://twiki.cern.ch/twiki/bin/viewauth/CMS/SummaryTable1G25ns#D

[56] The LHC Higgs cross-section working group. https://twiki.cern.ch/twiki/bin/view/LHCPhysics/LHCHXSWG.

[57] Standard Model Cross Sections for CMS at 13 TeV. https://twiki.cern.ch/twiki/bin/viewauth/CMS/StandardModelCrossSectionsat13TeVInclusi

[58] SM Higgs production cross sections at sqrt(s) = 13 TeV. https://twiki.cern.ch/twiki/bin/view/LHCPhysics/CERNYellowReportPageAt13TeV#ZHllH

[59] NNLO+NNLL top-quark-pair cross sections. https://twiki.cern.ch/twiki/bin/view/LHCPhysics/TtbarNNLO#Top_quark_pair_cross_se

[60] Single Top Cross sections. https://twiki.cern.ch/twiki/bin/viewauth/CMS/SingleTopSigma.

[61] CMS GEN XSEC Task Force. https://twiki.cern.ch/twiki/bin/viewauth/CMS/GenXsecTaskF

[62] SM Higgs Branching Ratios and Total Decay Widths (update in CERN Report4 2016). https://twiki.cern.ch/twiki/bin/view/LHCPhysics/CERNYellowReportPageBR#Higgs_2_g

[63] Ryan Gavin, Ye Li, Frank Petriello, and Seth Quackenbush. W Physics at the LHC with FEWZ 2.1. *Comput. Phys. Commun.*, 184:208, 2013.

[64] Stefano Frixione, Paolo Nason, and Giovanni Ridolfi. A Positive-weight next-to-leading-order Monte Carlo for heavy flavour hadroproduction. *JHEP*, 09:126, 2007.

[65] J. Alwall, R. Frederix, S. Frixione, V. Hirschi, F. Maltoni, O. Mattelaer, H. S. Shao, T. Stelzer, P. Torrielli, and M. Zaro. The automated computation of tree-level and next-to-leading order differential cross sections, and their matching to parton shower simulations. *JHEP*, 07:079, 2014.

[66] Gunter Zech. Upper Limits in Experiments with Background Or Measurement Errors. *Nucl. Instrum. Meth.*, A277:608, 1989.

[67] A. L. Read. Presentation of search results: the CLs technique. *J. Phys. G: Nucl. Part. Phys.*, 28, 2002.

[68] Rikkert Frederix, Emanuele Re, and Paolo Torrielli. Single-top t-channel hadroproduction in the four-flavour scheme with POWHEG and aMC@NLO. *JHEP*, 09:130, 2012.

[69] Johan Alwall et al. Comparative study of various algorithms for the merging of parton showers and matrix elements in hadronic collisions. *Eur. Phys. J. C*, 53:473–500, 2008.

[70] Serguei Chatrchyan et al. Determination of jet energy calibration and transverse momentum resolution in CMS. *JINST*, 6:P11002, 2011.

[71] John M. Campbell and R. K. Ellis. MCFM for the Tevatron and the LHC. *Nucl. Phys. Proc. Suppl.*, 205-206:10, 2010.

[72] Emanuele Re. Single-top Wt-channel production matched with parton showers using the POWHEG method. *Eur. Phys. J.*, C71:1547, 2011.

[73] Gael L. Perrin, Pedro Fernandez Manteca. Muon Identification and Isolation Scale-Factors on 2016 Dataset. `https://indico.cern.ch/event/611558/contributions/2465881/attachments/1407735/2151747/TnP_06_02_2017.pdf`.

[74] CMS Muon POG. Tracking SFs on the full 2016 data. `https://twiki.cern.ch/twiki/bin/view/CMS/MuonWorkInProgressAndPagResults#Results_on_the_full_2016_data`.

[75] Gael L. Perrin. Double Muon trigger efficiency per-leg approach. `https://indico.cern.ch/event/636555/contributions/2577291/attachments/1453162/2241537/TnP_DoubleMuSF_03_05_17.pdf`.

[76] Grace Dupuis. Collider Constraints and Prospects of a Scalar Singlet Extension to Higgs Portal Dark Matter. *JHEP*, 07:008, 2016.

[77] Oleg Antipin, David Atwood, and Amarjit Soni. Search for RS gravitons via W(L)W(L) decays. *Phys. Lett.*, B666:155–161, 2008.

[78] A. Liam Fitzpatrick, Jared Kaplan, Lisa Randall, and Lian-Tao Wang. Searching for the Kaluza-Klein Graviton in Bulk RS Models. *JHEP*, 09:013, 2007.

[79] Kaustubh Agashe, Hooman Davoudiasl, Gilad Perez, and Amarjit Soni. Warped Gravitons at the LHC and Beyond. *Phys. Rev.*, D76:036006, 2007.

[80] CMS Higgs PAG. List of question for the preapproval checks. `https://twiki.cern.ch/twiki/bin/viewauth/CMS/HiggsWG/HiggsPAGPreapprovalChecks`.

[81] CMS BTV POG. Supported Algorithms and Operating Points. `https://twiki.cern.ch/twiki/bin/viewauth/CMS/BtagRecommendation80XReReco#Supported_Algorithms_and_Operati`.

[82] Albert M Sirunyan et al. Search for resonant and nonresonant Higgs boson pair production in the bblnulnu final state in proton-proton collisions at sqrt(s) = 13 TeV. 2017.

[83] Abdus Salam and John Clive Ward. On a gauge theory of elementary interactions. *Nuovo Cim.*, 19:165–170, 1961.

[84] Steven Weinberg. A model of leptons. *Phys.Rev.Lett.*, 19:1264–1266, 1967.

[85] Albert M Sirunyan et al. Evidence for the Higgs boson decay to a bottom quark-antiquark pair. 2017.

[86] Albert M Sirunyan et al. Particle-flow reconstruction and global event description with the CMS detector. *JINST*, 12(10):P10003, 2017.

[87] Aruna Kumar Nayak. Reconstruction of physics objects in the CMS detector. *PoS*, CHARGED2012:010, 2012.

[88] Lisa Randall and Raman Sundrum. Large mass hierarchy from a small extra dimension. *Phys. Rev. Lett.*, 83:3370–3373, Oct 1999.

[89] Serguei Chatrchyan et al. Observation of a new boson at a mass of 125 GeV with the CMS experiment at the LHC. *Phys. Lett.*, B716:30–61, 2012.

[90] Georges Aad et al. Observation of a new particle in the search for the Standard Model Higgs boson with the ATLAS detector at the LHC. *Phys. Lett.*, B716:1–29, 2012.

[91] Giuliano Panico. Prospects for double Higgs production. *Frascati Phys. Ser.*, 61:102, 2016.

[92] I. Belotelov, I. Golutvin, D. Bourilkov, A. Lanyov, E. Rogalev, M. Savina, and S. Shmatov. Search for ADD extra dimensional gravity in di-muon channel with the CMS detector. CMS Note 2006/076, 2006.

[93] M. Aldaya, P. Arce, J. Caballero, B. de la Cruz, P. Garcia-Abia, J. M. Hernandez, M. I. Josa, and E. Ruiz. Discovery potential and search strategy for the standard model Higgs boson in the $H \to ZZ^{\star} \to 4\mu$ decay channel using a mass-independent analysis. CMS Note 2006/106, 2006.

[94] A. Brandt et al. Measurements of single diffraction at $\sqrt{s} = 630$ GeV: Evidence for a non-linear $\alpha(t)$ of the pomeron. *Nucl. Phys. B*, 514:3, 1998.

[95] W. Buchmüller and D. Wyler. Constraints on SU(5)-type leptoquarks. *Phys. Lett. B*, 177:377, 1986.

[96] CMS Collaboration. CMS technical design report, volume II: Physics performance. *J. Phys. G*, 34:995, 2007.

[97] CMS Collaboration. Jet performance in pp collisions at $\sqrt{s}$=7 TeV. CMS Physics Analysis Summary CMS-PAS-JME-10-003, 2010.

[98] S. Chatrchyan et al. The CMS experiment at the CERN LHC. *JINST*, 3:S08004, 2008.

[99] Particle Data Group, J. Beringer, et al. Review of Particle Physics. *Phys. Rev. D*, 86:010001, 2012.

[100] ALEPH, CDF, D0, DELPHI, L3, OPAL, SLD Collaborations, the LEP Electroweak Working Group, the Tevatron Electroweak Working Group, and the SLD Electroweak and Heavy Flavour Groups. Precision electroweak measurements and constraints on the Standard Model. 2010.

[101] I. Bertram, G. Landsberg, J. Linnemann, R. Partridge, M. Paterno, and H. B. Prosper. A recipe for the construction of confidence limits. Technical Report TM-2104, Fermilab, 2000.

[102] L. Moneta, K. Belasco, K. S. Cranmer, A. Lazzaro, D. Piparo, G. Schott, W. Verkerke, and M. Wolf. The RooStats Project. In *$13^{th}$ International Workshop on Advanced Computing and Analysis Techniques in Physics Research (ACAT2010)*. SISSA, 2010. PoS(ACAT2010)057.

[103] Vardan Khachatryan et al. Search for the standard model Higgs boson produced through vector boson fusion and decaying to $b\bar{b}$. *Phys. Rev.*, D92(3):032008, 2015.

[104] Performance of muon identification in pp collisions at s**0.5 = 7 TeV. Technical Report CMS-PAS-MUO-10-002, CERN, Geneva, 2010.

[105] Serguei Chatrchyan et al. Performance of CMS muon reconstruction in $pp$ collision events at $\sqrt{s} = 7$ TeV. *JINST*, 7:P10002, 2012.

[106] CMS COLLABORATION. Particle–flow event reconstruction in CMS and performance for jets, taus, and $E_T^{miss}$. CMS Physics Analysis Summary CMS-PAS-PFT-09-001, CERN, 2009.

[107] CMS COLLABORATION. Commissioning of the particle-flow event reconstruction with the first lhc collisions recorded in the cms detector. CMS Physics Analysis Summary CMS-PAS-PFT-10-001, CERN, 2010.

[108] Vardan Khachatryan et al. Performance of Electron Reconstruction and Selection with the CMS Detector in Proton-Proton Collisions at $\sqrt{s} = 8$ TeV. *JINST*, 10(06):P06005, 2015.

[109] CMS Collaboration. Search for pair production of first-generation scalar leptoquarks in pp collisions at $\sqrt{s} = 7$ TeV. Submitted to *Phys. Rev. Lett.*, 2010.

[110] CMS Collaboration. Performance of cms muon reconstruction in pp collision events at $\sqrt{s} = 7\,$TeV. Submitted to *J. Inst.*, 2012.

[111] ATLAS Collaboration. Search for the Higgs boson in the $H \rightarrow$WW(*)$\rightarrow \ell^+\nu\ell^-\bar{\nu}$ decay channel in pp collisions at $\sqrt{s} = 7$ TeV with the ATLAS detector. Submitted to *Phys. Rev. Lett.*, 2011.

[112] Matteo Cacciari and Gavin P. Salam. Dispelling the $N^3$ myth for the $k_t$ jet-finder. *Phys. Lett. B*, 641:57, 2006.

[113] CMS Luminosity Measurements for the 2016 Data Taking Period. Technical Report CMS-PAS-LUM-17-001, CERN, Geneva, 2017.

[114] CMS Muon POG. Reference muon id, isolation and trigger efficiencies for Run-II. `https://twiki.cern.ch/twiki/bin/viewauth/CMS/MuonReferenceEffsRun2`.

[115] John M. Campbell, R. Keith Ellis, Paolo Nason, and Emanuele Re. Top-pair production and decay at NLO matched with parton showers. *JHEP*, 04:114, 2015.

[116] Ryan Gavin, Ye Li, Frank Petriello, and Seth Quackenbush. FEWZ 2.0: A code for hadronic Z production at next-to-next-to-leading order. *Comput. Phys. Commun.*, 182:2388, 2011.

[117] Ye Li and Frank Petriello. Combining QCD and electroweak corrections to dilepton production in FEWZ. *Phys. Rev. D*, 86:094034, 2012.

[118] Vardan Khachatryan et al. Event generator tunes obtained from underlying event and multiparton scattering measurements. *Eur. Phys. J. C*, 76(3):155, 2016.

[119] Torbjorn Sjostrand, Stephen Mrenna, and Peter Z. Skands. A Brief Introduction to PYTHIA 8.1. *Comput. Phys. Commun.*, 178:852–867, 2008.

[120] Rikkert Frederix and Stefano Frixione. Merging meets matching in MC@NLO. *JHEP*, 12:061, 2012.

[121] Simone Alioli, Paolo Nason, Carlo Oleari, and Emanuele Re. NLO single-top production matched with shower in POWHEG: s- and t-channel contributions. *JHEP*, 09:111, 2009. [Erratum: JHEP02,011(2010)].

[122] Michele de Gruttola, Caterina Vernieri, Pierluigi Bortignon, David Curry, Ivan Furic, Jacobo Konigsberg, Sean-Jiun Wang, Paolo Azzurri, Tommaso Boccali, Andrea Rizzi, Silvio Donato, Stephane Brunet Cooperstein , James Olsen, Christopher Palmer, Lorenzo Bianchini, Christoph Grab, Gael Ludovic Perrin, and Luca Perrozzi. Search for the Standard Model Higgs Boson Produced in Association with W and Z and Decaying to Bottom Quarks. http://cms.cern.ch/iCMS/jsp/db_notes/noteInfo.jsp?cmsnoteid=CMS%20AN-2015/168.

[123] Michele de Gruttola, Rami Kamalieddin, Ilya Kravchenko, Lesya Shchutska. Search for resonant diHiggs production with bbZZ decays with the 2b2l2nu signature using 35.9/fb data of 2016 pp collisions at the LHC. http://cms.cern.ch/iCMS/jsp/openfile.jsp?tp=draft&files=AN2017_198_v17.pdf.

[124] Chris Palmer. VHbb Electron Trigger and ID+ISO SFs for 2016 data. https://indico.cern.ch/event/604949/contributions/2543520/attachments/1439974/2216426/VHbb_TnP_SFs_egamma_april.pdf#search=vhbb%20AND%20cerntaxonomy%3A%22Indico%2FExperiments%2FCMS%20meetings%2FPH%20%2D%20Physics%2FEgamma%22.

[125] CMS JetMET group. Jet Energy Resolution. https://twiki.cern.ch/twiki/bin/viewauth/CMS/JetResolution.

[126] CMS MET group. MET Corrections and Uncertainties for Run-II. https://twiki.cern.ch/twiki/bin/viewauth/CMS/MissingETRun2Corrections.

[127] CMS MET group. MET Filter Recommendations for Run II. `https://twiki.cern.ch/twiki/bin/view/CMS/MissingETOptionalFiltersRun2`.

[128] CMS EGM POG. Multivariate Electron Identification for Run2. `https://twiki.cern.ch/twiki/bin/viewauth/CMS/Multivari\ateElectronIdentificationRun2`.

[129] Helge Voss, Andreas Höcker, Jörg Stelzer, and Frerik Tegenfeldt. TMVA, the toolkit for multivariate data analysis with ROOT. In *XIth International Workshop on Advanced Computing and Analysis Techniq ues in Physics Research (ACAT)*, page 40, 2007.

[130] CMS Higgs WG. Documentation of the RooStats -based statistics tools for Higgs PAG. `https://twiki.cern.ch/twiki/bin/view/CMS/SWGuideHiggsAnalysisCombinedLimit`.

[131] CMS Higgs WG. Binned shape analysis with the Higgs Combination Tool. `https://twiki.cern.ch/twiki/bin/view/CMS/SWGuideHiggsAnalysisCombinedLimit#Binned_shape_analysis`.

[132] bbbb team. Search for resonant pair production of Higgs bosons decaying to bottom quark-antiquark pairs in proton-proton collisions at 13 TeV. `http://cms.cern.ch/iCMS/analysisadmin/get?analysis=HIG-17-009-pas-v5.pdf`.

[133] Matteo Cacciari, Gavin P. Salam, and Gregory Soyez. The anti-$k_t$ jet clustering algorithm. *JHEP*, 04:063, 2008.

[134] Torbjörn Sjöstrand, Stephen Mrenna, and Peter Skands. PYTHIA 6.4 physics and manual. *JHEP*, 05:026, 2006.

[135] C. Giunti and M. Laveder. Neutrino mixing. In F. Columbus and V. Krasnoholovets, editors, *Developments in Quantum Physics*. Nova Science Publishers, Inc., 2004.

[136] Savas Dimopoulos, Stuart Raby, and Frank Wilczek. Proton decay in supersymmetric models. *Physics Letters B*, 112(2):133 – 136, 1982.

[137] M. Della Negra, P. Jenni, and T. S. Virdee. Journey in the search for the higgs boson: The atlas and cms experiments at the large hadron collider. *Science*, 338(6114):1560–1568, 2012.

[138] Thomas Schörner-Sadenius. *The Large Hadron Collider: harvest of run 1*. Springer, Cham, 2015.

[139] CERN. *Large Hadron Collider in the LEP Tunnel*, Geneva, 1984. CERN.

[140] Lyndon R Evans and Philip Bryant. LHC Machine. *JINST*, 3:S08001. 164 p, 2008. This report is an abridged version of the LHC Design Report (CERN-2004-003).

[141] Karsten Eggert, K Honkavaara, and Andreas Morsch. Luminosity considerations for the LHC. Technical Report CERN-AT-94-04-DI. CERN-LHC-Note-263. LHC-NOTE-263, CERN, Geneva, Feb 1994.

[142] Oswald Gröbner. The LHC Vacuum System. (LHC-Project-Report-181. CERN-LHC-Project-Report-181):5 p, May 1998.

[143] Wolfgang Adam, R Frühwirth, Are Strandlie, and T Todor. Reconstruction of Electrons with the Gaussian-Sum Filter in the CMS Tracker at the LHC. Technical Report CMS-NOTE-2005-001, CERN, Geneva, Jan 2005.

[144] Thomas Lenzi. Development and Study of Different Muon Track Reconstruction Algorithms for the Level-1 Trigger for the CMS Muon Upgrade with GEM Detectors. Master's thesis, U. Brussels (main), 2013.

[145] Prospects for HH measurements at the HL-LHC. Technical Report CMS-PAS-FTR-18-019, CERN, Geneva, 2018.

[146] Combination of searches for Higgs boson pair production in proton-proton collisions at $\sqrt{s} = 13$ TeV. Technical Report CMS-PAS-HIG-17-030, CERN, Geneva, 2018.

[147] The CMS collaboration. Missing transverse energy performance of the cms detector. *Journal of Instrumentation*, 6(09):P09001, 2011.

[148] Search for resonant double Higgs production with $bbZZ$ decays in the $b\bar{b}\ell\ell\nu\nu$ final state. Technical Report CMS-PAS-HIG-17-032, CERN, Geneva, 2018.